Development of mutated β-catenin gene signature to identify *CTNNB1* mutations from whole and spatial transcriptomic data in patients with HCC

Brandon M. Lehrich, Junyan Tao, Silvia Liu, Theo Z. Hirsch, Tyler M. Yasaka, Catherine Cao, Evan R. Delgado, Xiangnan Guan, Shan Lu, Long Pan, Yuqing Liu, Sucha Singh, Minakshi Poddar, Aaron Bell, Aatur D. Singhi, Jessica Zucman-Rossi, Yulei Wang, Satdarshan P. Monga

Table of contents

Materials and methods……2

Supplementary figures……11

Supplementary tables S1-8……separate excel file

Table S9……57

Supplementary references……64

Materials and methods

Plasmids

We have previously described the S45Y-CTNNB1-Myc-tag plasmid.[1] Briefly, using PCR-based site-directed mutagenesis, the S45Y substitution is introduced into human WT-CTNNB1-Myc-tag-bearing plasmid and subcloned into pT3-EF5αh plasmid using Gateway PCR cloning technology (Invitrogen, Carlsbad, CA) (pT3-EF5αh-S45Y-CTNNB1-Myc-tag). G31A-mutated human NFE2L2 was previously purchased from Addgene (catalog #81524) as a Gateway donor vector and subcloned into pT3-EF1αh destination vector (pT3-EF1αh-G31A-NFE2L2) as previously described.[2] The pT3-EF5αh-hMet-V5-tag and pCMV/SB transposase plasmid have been described previously.[1, 3] All these plasmid constructs were purified using Endotoxin-Free Maxiprep kit (NA 0410, Sigma-Aldrich, St. Louis, MO) for hydrodynamic delivery. For hydrodynamic delivery, plasmids were diluted in 0.9% normal saline (NaCl) purchased from TEKNOVA (#S5815).

Mice for Tumor Study

All FVB/N mice used for tumor study were purchased from the Jackson Laboratory (Bar Harbor, ME). All procedures were performed in accordance with and approved by University of Pittsburgh School of Medicine Institutional Animal Use and Care Committee. All mice were fed a standard chow diet *ad libitum*, water, had access to enrichment, and exposed to 12h light/dark cycles in ventilated cages. Mice were monitored for signs of abdominal girth, morbidity, and were euthanized appropriately. All mice were euthanized at the indicated timepoints. Prior to sacrifice, mice were fasted for 4-6 hours. Body and liver weights were measured, along with documenting

the gross morphology of the mouse livers at time of tissue harvesting. Kaplan Meier survival curve was generated using Prism 8 software (GraphPad Software Inc., La Jolla, CA).

Hydrodynamic Tail Vein Gene Delivery

The SB-HDTVI model has been described previously.[1-4] For the CTNNB1-mutated/NRF2/hMET model (β-N-M), 20μg of pT3-EF5αh-S45Y-CTNNB1-Myc-tag, 20μg of NFE2L2-plasmid (pT3-EF1αh-G31A-NFE2L2), and 20μg of hMET-plasmid (pT3-EF5αh-hMet-V5-tag) were mixed. For the CTNNB1-mutated/hMET model (β-M), 20μg of pT3-EF5αh-S45Y-CTNNB1-Myc-tag and 20μg of hMET-plasmid (pT3-EF5αh-hMet-V5-tag) were mixed. For the CTNNB1-mutated/NRF2 model (β-N), 20μg of pT3-EF5αh-S45Y-CTNNB1-Myc-tag and 20μg of NFE2L2-plasmid (pT3-EF1αh-G31A-NFE2L2) were mixed. For the NRF2/hMET model (N-M), 20μg of NFE2L2-plasmid (pT3-EF1αh-G31A-NFE2L2) and 20μg of hMET-plasmid (pT3-EF5αh-hMet-V5-tag) were mixed. Each of these plasmid combinations were additionally mixed with pCMV/SB transposase plasmid at a concentration of 25:1 in 2ml normal saline (0.9% NaCl) and filtered through 0.22 um filter (Millipore) for injection. For hydrodynamic delivery, 6–8-week-old FVB/N male mice were injected in the lateral tail vein in 5-7 seconds.

The Hematoxylin and eosin (H&E) staining

Liver tissue chunks were fixed with 10% buffered formalin (Fisher Chemicals) at room temperature for 48-72h. Liver tissue is then transferred to 70% ethanol for tissue dehydration and paraffin embedding (FFPE) in blocks. The FFPE blocks are cut to 4μm sections for tissue staining. Standard workflow was used for hematoxylin and eosin (H&E) stain (Fisher Chemical Harris Modified Method Hematoxylin Stains, #SH26-500D; Eosin Y, # 23-314-630; ThermoFisher

Scientific, Waltham, MA). This allowed identification and characterization of neoplastic foci in liver tissue sections.

Histology and Immunohistochemistry (IHC)

For IHC, FFPE sections underwent deparaffinization in xylene, followed by serial deparaffinization in stepwise decreases in ethanol (100%, 95%, 90%) and rinsed in water. Antigen retrieval consisted of either Citrate Buffer (0.01 M, pH 6.0), or Tris-EDTA (1X Tris-EDTA Buffer, pH 9.0), or DAKO reagent (Agilent, Santa Clara, CA). Slides were then heated by either microwave for total of 18 minutes or under high pressure and temperature (via pressure cooker) for 20 minutes. Slides were then cooled on ice for 30-45mins. Slides were then incubated in 3% H_2O_2 dissolved in 1X phosphate-buffered saline (PBS) for 10 minutes to quench endogenous liver peroxidases. Slides were then washed in PBS 3x. Next, sections were blocked with Super Block (ScyTek Laboratories) for 10min to prevent non-specific binding. Slides were then incubated with the following antibodies at room temperature for 1h at indicated dilutions: glutamine synthetase (#G2781, Sigma-Aldrich; 1:1500), Cyclin-D1 (#134175, Abcam; 1:100), Ki67 (#cs12202; Cell Signaling; 1:500), or β-catenin (#BD610154; BD BioSciences; 1:100); Or, at cold temperature overnight: NQO1 (#sc-376023, Santa Cruz; 1:100), Myc-tag (#cs-2278; Cell Signaling; 1:100), or V5-tag (#eBioSci-14-6796-82; eBioSciences; 1:100). Next, slides were then washed with 1x PBS 3x and then incubated with species-specific biotinylated secondary antibodies (EMD Millipore) for 30 mins at room temperature. Next, slides were then washed with 1x PBS 3x and then incubated with ABC reagent (Vectastain ABC Elite kit, Vector Laboratories) for 15 minutes. Then, slides were washed with 1x PBS 3x and then brown stain signal was observed with incubation with DAB Peroxidase Substrate Kit (Vector Laboratories) for 30 seconds to 2mins. Last, slides were

counterstained with hematoxylin (ThermoFisher Scientific), and rinsed, then dehydrated, mounted, and cover slipped. Slides were imaged on Zeiss Axioskop microscope and analyzed in Adobe Photoshop CS6 (Version 13.0 x64).

RNA-Sequencing and Analysis and development of MBGS

Using fresh frozen liver tissue, RNA was isolated using the RNeasy Mini kit (Qiagen) according to standard manufacturer protocols for tissue RNA isolation and as previously described.[1, 4] RNA sequencing was performed on 15 mice for this study: 3 mice wild-type, 3 mice from S45Y-CTNNB1/G31A-NFE2L2/hMET (β-N-M), 3 mice from S45Y-CTNNB1/hMET (β-M), 3 mice from S45Y-CTNNB1/G31A-NFE2L2 (β-N), and 3 mice from G31A-NFE2L2/hMET (N-M). Transcriptome sequencing, quality control, and data preprocessing was performed as previously described.[2] The RNA-seq data is deposited to Gene Expression Omnibus (GEO) under accession number: **GSE261316**.

To identify differentially expressed genes (DEGs) between each of the models and wild-type liver and between different models, differential expression analysis was performed in R using the R package 'DEseq2' using total gene counts. DEGs were selected based on absolute log fold-change greater than 1.5 and FDR=0.05. These DEGs were then further used for input to Ingenuity Pathway Analysis (IPA)® (Qiagen) to enrich for pathways with biological meaning (FDR=0.1). To further refine the DEGs between β-catenin-mutated and β-catenin-wild-type models, we used absolute log fold-change greater than 3 and FDR=0.05 as the threshold criteria for up and downregulated DEGs with each of the 3 comparisons. Mouse genes were mapped 1:1 to human orthologs using 'biomaRT' R package. The 95 upregulated mouse genes mapped to 85 human orthologs. To define MBGS with human HCC TCGA-LIHC data, DGE analysis was performed

on the 85 genes using absolute log fold-change greater than 3 and FDR=0.05 as the threshold criteria. This narrowed the gene list to 13-genes (MBGS). Inspection of expression of each individual gene in NTL, CTNNB1-mutated, and CTNNB1-wild-type narrowed the gene list to 10-genes (modified MBGS).

Human HCC Data Mining

For The Cancer Genome Atlas (TCGA) Liver Hepatocellular Carcinoma (TCGA-LIHC) analysis, RNA-seq transcriptomic and whole exome sequencing data were downloaded from Genomic Data Commons (GDC) through the R Bioconductor package 'GenomicDataCommons'. Gene counts were normalized and the R package 'DEseq2' was used to determine differentially expressed genes (DEGs). DEGs were defined based on FDR and absolute log fold change thresholds and used for Ingenuity Pathway Analysis (IPA)® (Qiagen) for inferred biological meaning. For patient stratification by gene signature overlap, we used the previously published NRF2 activation gene signature[5] and the KAPOSI_LIVER_CANCER_MET_UP gene signature from mSigDB.[6] Patients were hierarchically clustered based on high/low expression of the gene signature and patients with high expression of each were defined as NRF2/MET-high patients. Those patients that were also CTNNB1-mutated based on exome sequencing, where defined as CTNNB1-mutated/NRF2/MET-high. Lollipop plots for CTNNB1 gene were generated using cBioPortal MutationMapper online tool (https://www.cbioportal.org/mutation_mapper). Additionally, we performed analysis in a separate French cohort which contained genomic data (Whole-Genome Sequencing, Whole Exome Sequencing and RNAseq) from 398 adult HCC, 100 hepatoblastomas, 34 hepatocellular adenomas and 31 non-tumor liver samples previously sequenced (EGA accession numbers EGAS00001001284, EGAS00001002091,

EGAS00001002879, EGAS00001003025, EGAS00001003310, EGAS00001003685, EGAS00001003837, EGAS00001004629, EGAS00001005108, EGAS00001005986, EGAS00001006692, EGAS00001001002, EGAS00001000217, EGAS00001005629, EGAS00001003063, EGAS00001000706, EGAS00001003130, EGAS00001002408, EGAS00001002888, EGAS00001000679 and EGAS00001003686) and we annotated all *CTNNB1* activating mutations or deletions as well as *APC* biallelic inactivation. Moreover, MBGS predictive ability was tested in a small immunotherapy HCC cohort (n=8 responders; n=9 non-responders) (GSE202069). Following differential gene expression analysis, average normalized expression values were calculated for each of the genes in 10-gene MBGS and composite score, along with calculation of ROC AUC values for each. Additionally, MBGS was compared against Chiang CTNNB1 subclass gene signature for ICI response, and other ICI response gene signatures, including T cell-inflamed gene expression profile ("CCL5", "CD27", "CD274", "CD276", "CD8A", "CMKLR1", "CXCL9", "CXCR6", "HLA-DQA1", "HLA-DRB1", "HLA-E", "IDO1", "LAG3", "NKG7", "PDCD1LG2", "PSMB10", "STAT1"), IFNg response signature ("CXCL10", "CXCL9", "HLA-DRA", "IDO1", "IFNG", "STAT1"), and tertiary lymphoid structure (TLS) signature ("CCL19", "CCL21", "CXCL13", "CCR7", "SELL", "LAMP3", "CXCR4", "CD86", "BCL6"). Lastly, we retrospectively analyzed clinical, genomic, and transcriptomic data (Whole Exome Sequencing and RNAseq data) from IMbrave150 trial[7] for expression of our 10- and 13-gene MBGS signatures and association with clinical parameters (overall and progression-free survival and clinical response using mRECIST criteria).

To assess performance of MBGS in the pan-cancer atlas, genomic and transcriptomic data was accessed from cBioPortal.org using the “Pan-cancer analysis of whole genomes (ICGC/TCGA, Nature 2020)” dataset. ROC AUC value was calculated to predict CTNNB1

mutational status using 10-gene MBGS in this cohort. Additionally, performance of MBGS was compared to other molecular subclass gene signatures and Wnt gene signatures (accessed from MSigDB or the publications themselves), composite average expression of the different genes of the signature were computed and a logistic regression model was used to predict gene signature score with CTNNB1-mutation status. AUC and ROC curves were computed using R package 'pROC'. Sensitivity (True Positive Rate) and Specificity (True Negative Rate) values were determined using Youden's J statistic (sensitivity + specificity – 1) to define the best fit threshold for these values on the ROC curve. Boxplots were used to compare composite average expression across the normal liver, CTNNB1-mutated, and CTNNB1-wild-type cases. Gene signatures and their definitions (gene lists) are listed in the Online **Supplemental Table 9**.

Human HCC Molecular Subclassification of TCGA data

To define TCGA-LIHC patients according to Hoshida[8], Boyault[10], and Chiang[9] molecular subclasses for heatmap representation, we used the 'MS.liverK' R package[13] downloaded from https://github.com/cit-bioinfo/MS.liverK. Following data conversion step since the package algorithm was meant to be used on microarray dataset, we followed the package vignette to categorize all the TCGA-LIHC cases (including adjacent normal) into the different molecular subclasses using normalized data. Data was exported as .csv file and used to generate heatmap.

Human HCC Spatial Transcriptomic Data Mining

We used two publicly available human HCC spatial transcriptomic (10X Visium) datasets[14, 15] to visualize expression of molecular subclass gene signatures and Wnt gene signatures

on the H&E tissue section. The Zhang et al. study data was accessed from gene expression omnibus (GSE238264) and the Wu et al. study data was accessed directly from http://lifeome.net/supp/livercancer-st/data.htm. Raw data was downloaded and all 12 patient 10X Visium slides were processed using the R package 'Seurat'.[16] Sequenced 55 μm spatial regions (spots) were filtered to exclude regions of low sequencing quality, using a threshold of 2000 reads per spot. Spots were subsequently normalized and integrated using Seurat. Additionally, as part of this quality control step, we decided not to proceed with analysis of slide 'HCC 2R' from Zhang et al. study since it did not have sufficient spots for analysis following this preprocessing step. Thus, we limited our analysis to 11 individual patient slides (across 12 total slides). The Wu et al. study contained typically 3 slides per patient (1 normal liver, 1 leading edge [tumor + normal], and 1 tumor region]. We limited analysis to just the tumor region slide, although all these slides were ultimately integrated in our Seurat object. Additionally, slide 5 in the Wu et al. study had only tumor regions, but there were 4 regions [labeled A-D]. The best quality data were from regions B-C, which was ultimately what the analysis was performed on.

Each of the molecular subclass signatures or Wnt gene signatures detailed in **Supplemental Table 9** were spatially plotted on the tissue section using the 'addGeneSig' function within the 'SpatialPlot' function of Seurat. We also filtered out genes from the 'addGeneSig' function that were expressed with fewer than 1 count in an individual spot. Due to sequencing depth, some genes in the signature may not have been analyzed. Lastly, all the module scores for a given molecular subclass or gene signature were normalized within each HCC patient slide.

Statistical Analysis

All data presented in the manuscript is depicted as mean ± standard deviation (SD) for each group. The indicated statistical tests were performed in Prism 9 software (GraphPad Software Inc., La Jolla, CA). For our study, $P < 0.05$ was considered statistically significant (*$p<0.05$, **$p<0.01$, ***$p<0.001$).

Supplementary figures

Fig. S1

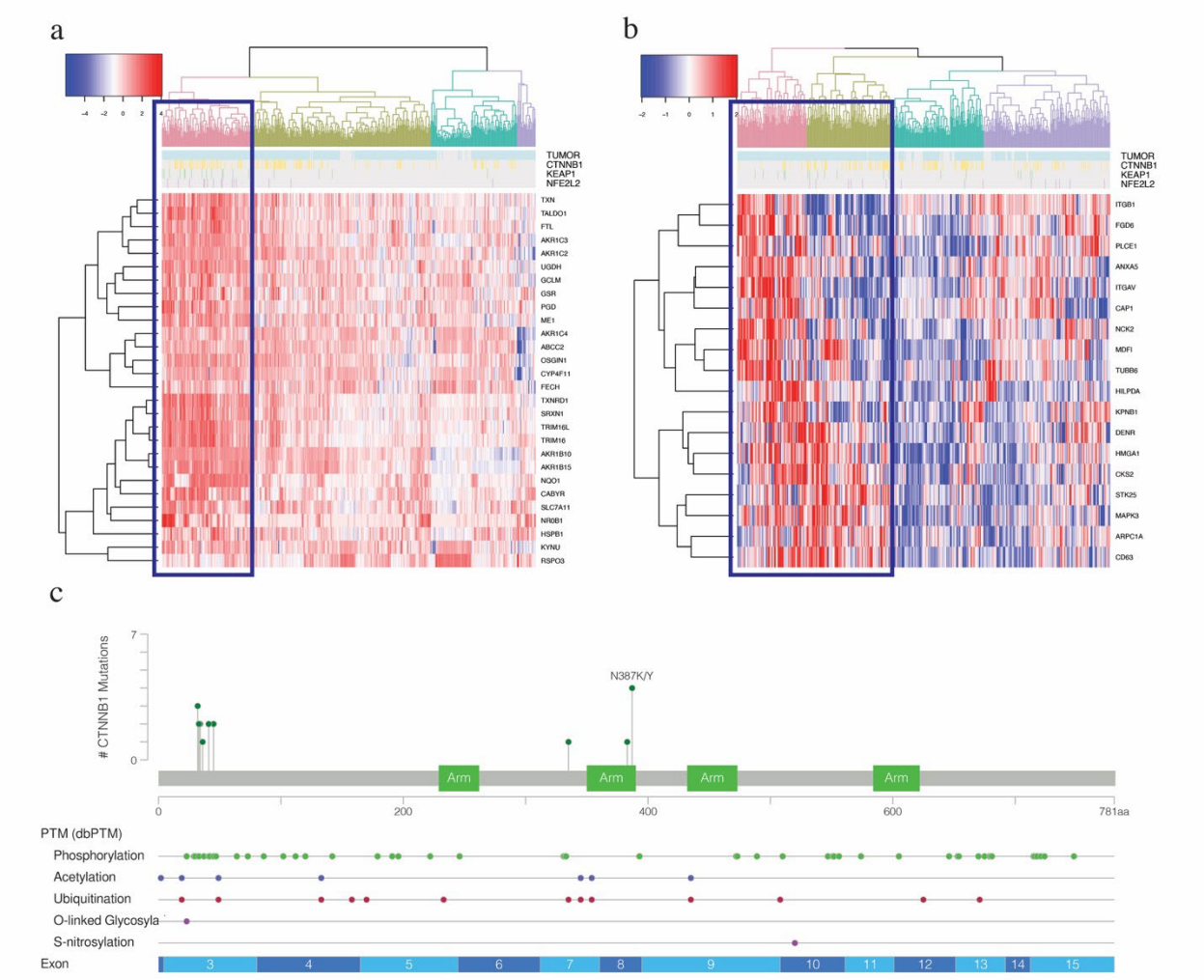

Fig. S1: CTNNB1 mutations occur in patients with high expression of NRF2 and MET gene signature. (A) Hierarchical clustering applied to TCGA-LIHC dataset (n=374 tumor; n=50 adjacent normal) for 28-gene NRF2 signature identifies 100 cases (pink cluster with blue box) with NRF2-activation (NRF2-high), of which all were tumor cases. (B) Hierarchical clustering applied to TCGA-LIHC dataset (n=374 tumor; n=50 adjacent normal) for 18-gene KAPOSI_LIVER_CANCER_MET_UP signature identifies 176 cases (pink and green clusters with blue box) with MET-activation (MET-high), of which 175 were tumor cases. For (A-B) Normalized and scaled gene expression values based on z-score is shown. (C) Lollipop plot depicting number of CTNNB1 mutations within each exon of CTNNB1 gene for the 18 patients with NRF2-/MET-high gene signature overlap and CTNNB1 mutation. Created in cBioPortal. Figure 1A has been modified from our previous study (Tao J, Krutsenko Y, Moghe A, et al. Nuclear factor erythroid 2-related factor 2 and beta-Catenin Coactivation in Hepatocellular Cancer: Biological and Therapeutic Implications. *Hepatology*. Aug 2021;74(2):741-759. doi:10.1002/hep.31730).

Fig. S2

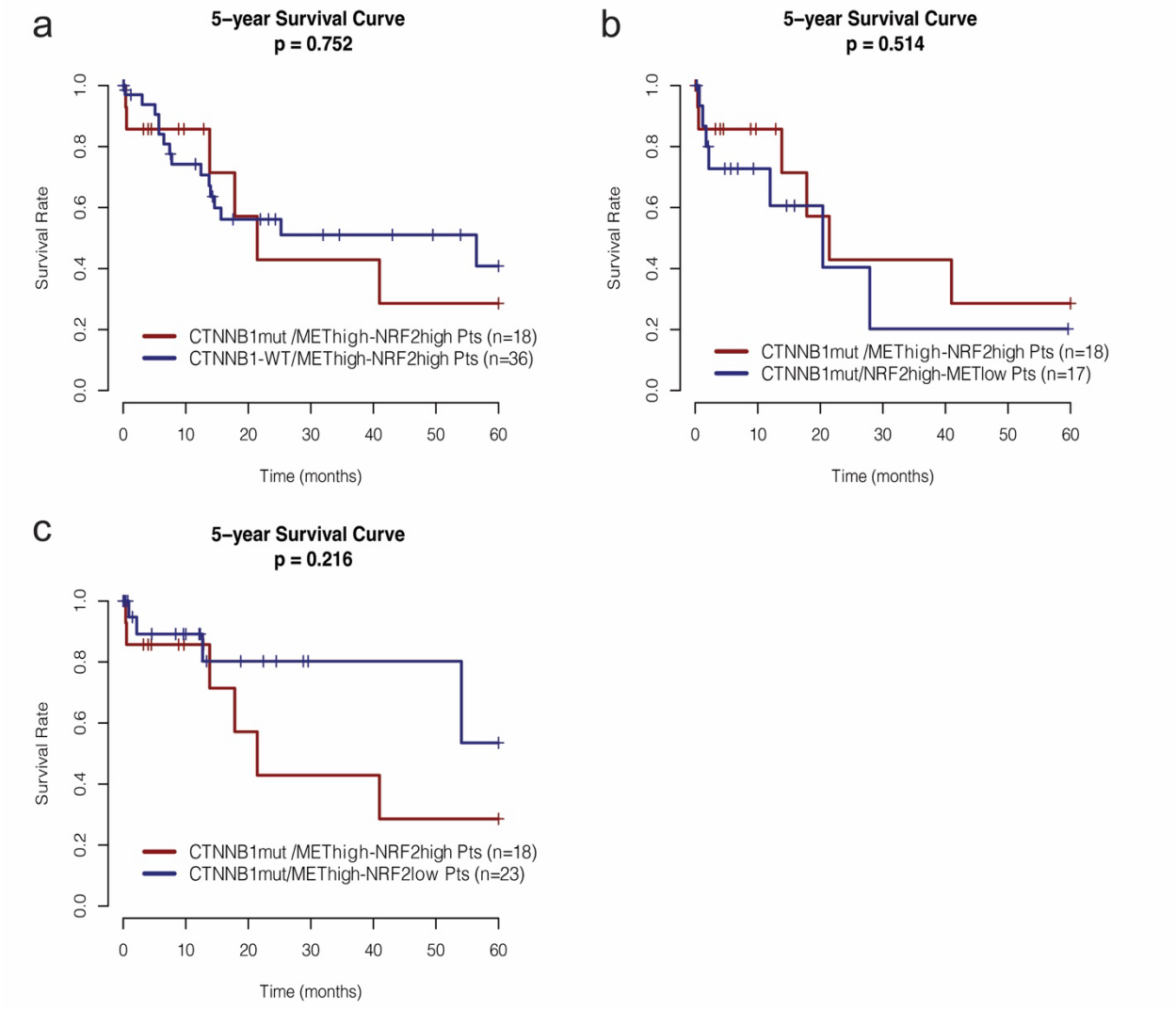
a
5–year Survival Curve
p = 0.752
Survival Rate
Time (months)
CTNNB1mut /METhigh-NRF2high Pts (n=18)
CTNNB1-WT/METhigh-NRF2high Pts (n=36)
b
5–year Survival Curve
p = 0.514
Survival Rate
Time (months)
CTNNB1mut /METhigh-NRF2high Pts (n=18)
CTNNB1mut/NRF2high-METlow Pts (n=17)
C
5–year Survival Curve
p = 0.216
Survival Rate
Time (months)
CTNNB1mut /METhigh-NRF2high Pts (n=18)
CTNNB1mut/METhigh-NRF2low Pts (n=23)

Fig. S2: NRF2/MET-high expression influences survival in CTNNB1-mutated patients, rather than CTNNB1-mutation influencing survival outcome. (A) Kaplan-Meier curve comparing CTNNB1-mut/NRF2-high/MET-high (n=18) vs CTNNB1-WT/NRF2-high/MET-high (n=36). Log-rank p-value is p=0.752. (B) Kaplan-Meier curve comparing CTNNB1-mut/NRF2-high/MET-high (n=18) vs CTNNB1-WT/NRF2-high/MET-low (n=17). Log-rank p-value is p=0.514. (C) Kaplan-Meier curve comparing CTNNB1-mut/NRF2-high/MET-high (n=18) vs CTNNB1-WT/NRF2-low/MET-high (n=23). Log-rank p-value is p=0.216. Additionally, Log-rank p-value is indicated on the Kaplan-Meier curve of 5-year overall survival. Levels of significance: *p<0.05, **p<0.001, ***p<0.0001.

Fig. S3

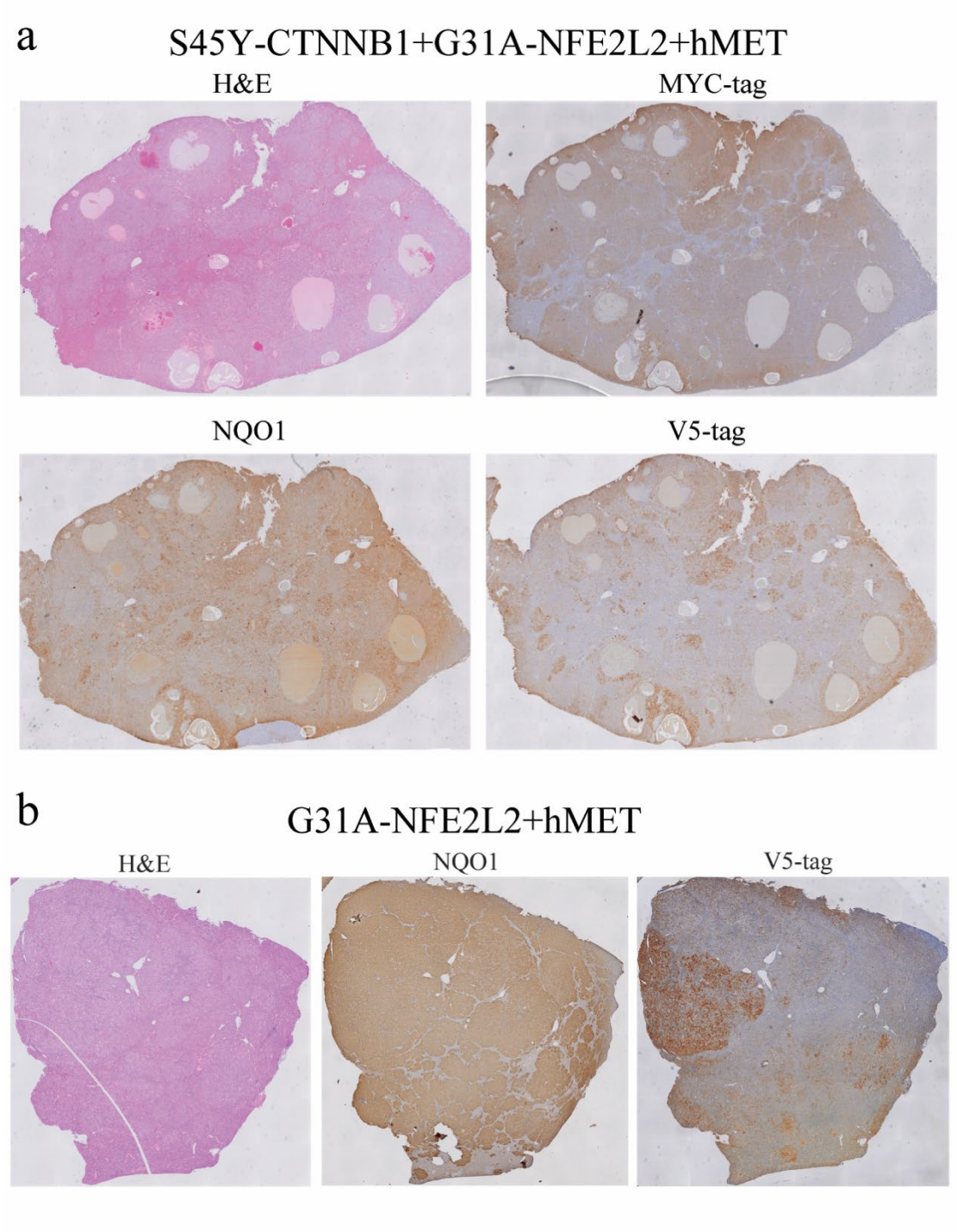
a
S45Y-CTNNB1+G31A-NFE2L2+hMET
H&E
MYC-tag
NQO1
V5-tag
b
G31A-NFE2L2+hMET
H&E
NQO1
V5-tag

Fig. S3: Forced expression of S45Y-CTNNB1 ± G31A-NFE2L2+hMET in mice induces HCC. (A) H&E tiled image of representative mouse liver, and representative tiled images for Myc-tag (present on mutant CTNNB1 plasmid), Nqo1 (downstream marker of Nqo1), and V5-tag (present on hMET plasmid) IHC for S45Y-CTNNB1 ± G31A-NFE2L2+hMET model. (B) Representative tiled images of H&E staining, Nqo1 (downstream marker of Nqo1), and V5-tag (present on hMET plasmid) IHC for G31A-NFE2L2+hMET model.

Fig. S4

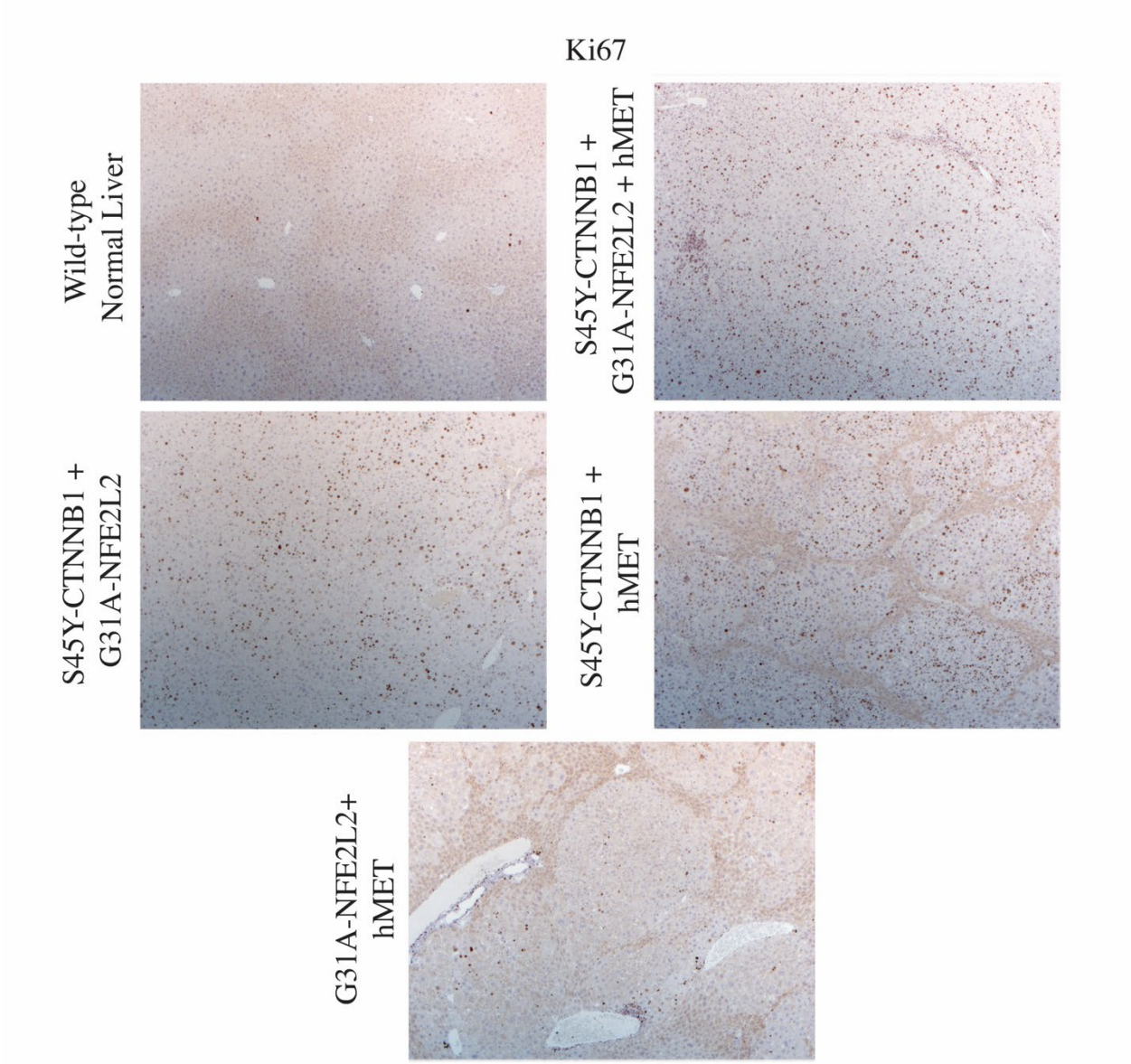
Ki67
Wild-type
Normal Liver
S45Y-CTNNB1 +
G31A-NFE2L2 + hMET
S45Y-CTNNB1 +
G31A-NFE2L2
S45Y-CTNNB1 +
hMET
G31A-NFE2L2+
hMET

Fig. S4: Characterization of cell proliferative markers in all murine HCC models.

Immunohistochemistry for Ki67 for wild-type liver, S45Y-CTNNB1+G31A-NFE2L2+hMET, S45Y-CTNNB1+hMET, S45Y-CTNNB1+G31A-NFE2L2, and G31A-NFE2L2+hMET. 5X objective magnification.

Fig. S5

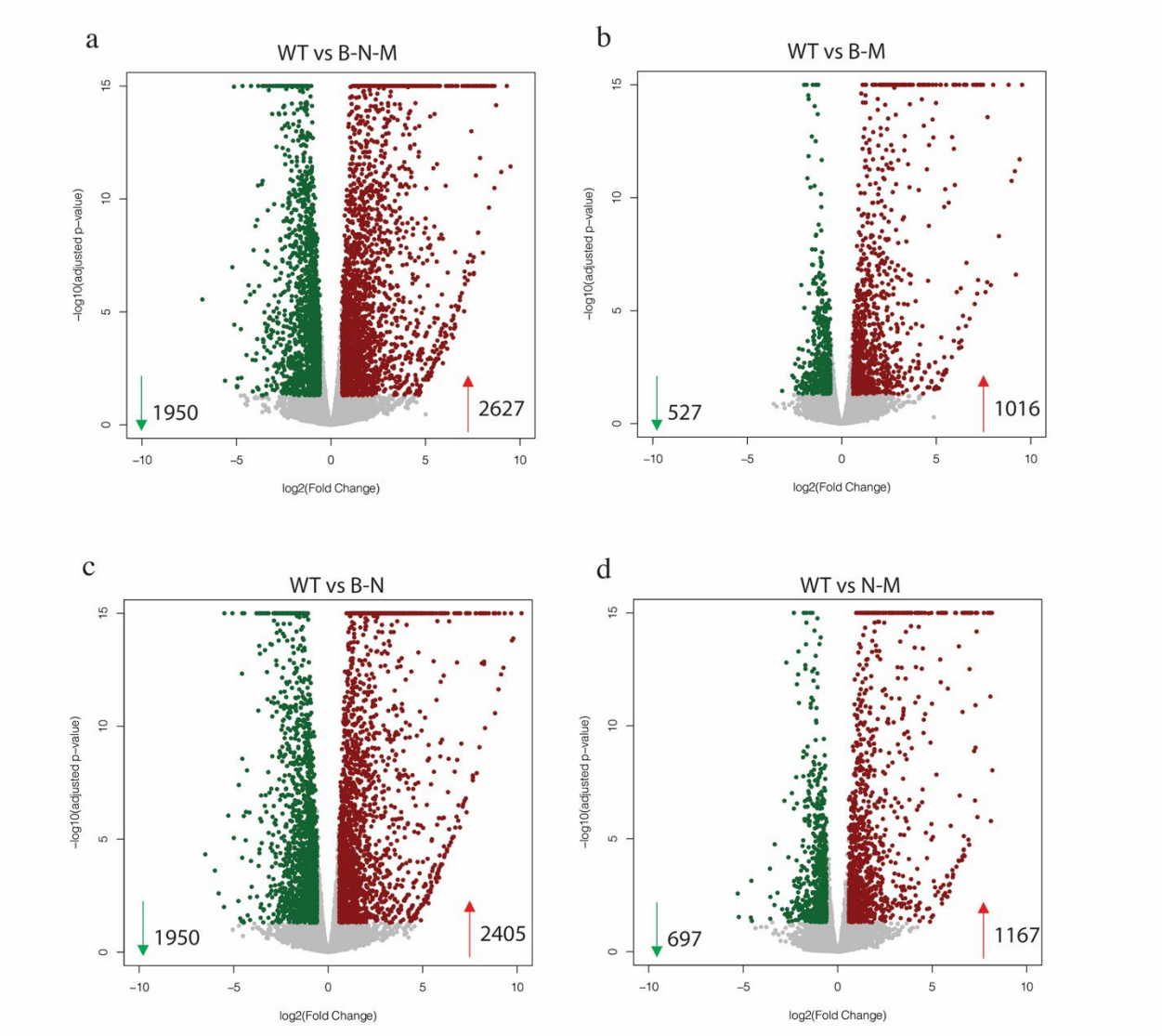
a
WT vs B-N-M
−log10(adjusted p−value)
log2(Fold Change)
1950
2627
b
WT vs B-M
−log10(adjusted p−value)
log2(Fold Change)
527
1016
c
WT vs B-N
−log10(adjusted p−value)
log2(Fold Change)
1950
2405
d
WT vs N-M
−log10(adjusted p−value)
log2(Fold Change)
697
1167

Fig. S5: Differential gene expression analysis comparing each tumor model to wild-type normal FVB liver. (A) Volcano plot illustrating 2627 upregulated and 1950 downregulated genes comparing WT vs β-N-M, (B) Volcano plot illustrating 1016 upregulated and 527downregulated genes comparing WT vs β-M, (C) Volcano plot illustrating 2405 upregulated and 1950 downregulated genes comparing WT vs β-N, and (D) Volcano plot illustrating 1167 upregulated and 697 downregulated genes comparing WT vs N-M. Differential gene expression analysis was performed with cutoff of FDR=0.05 and absolute log fold change > 1.5.

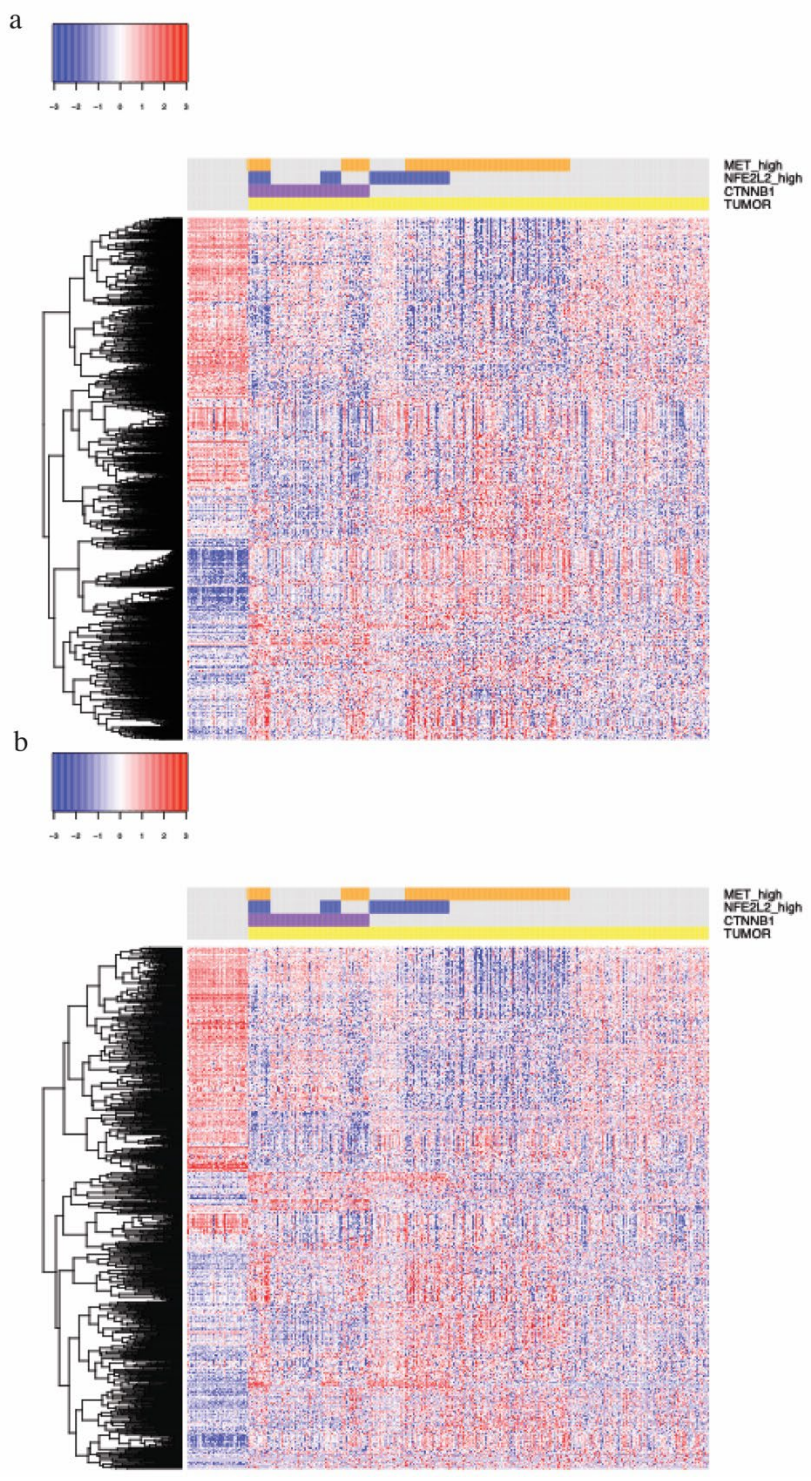
a
MET_high
NFE2L2_high
CTNNB1
TUMOR
b
MET_high
NFE2L2_high
CTNNB1
TUMOR

Fig. S6

Fig. S6: Common differentially expressed genes in mouse and human HCC with similar molecular perturbations. (A) Heatmap of common 2,377 differentially expressed genes in mouse WT vs β-N-M and human normal liver (NL) vs CTNNB1-mutant/NRF2-/MET-high. A) Heatmap of common 970 differentially expressed genes in mouse WT vs N-M and human NL vs NRF2-/MET-high. Normalized scaled gene expression based on z-score is shown.

Fig. S7

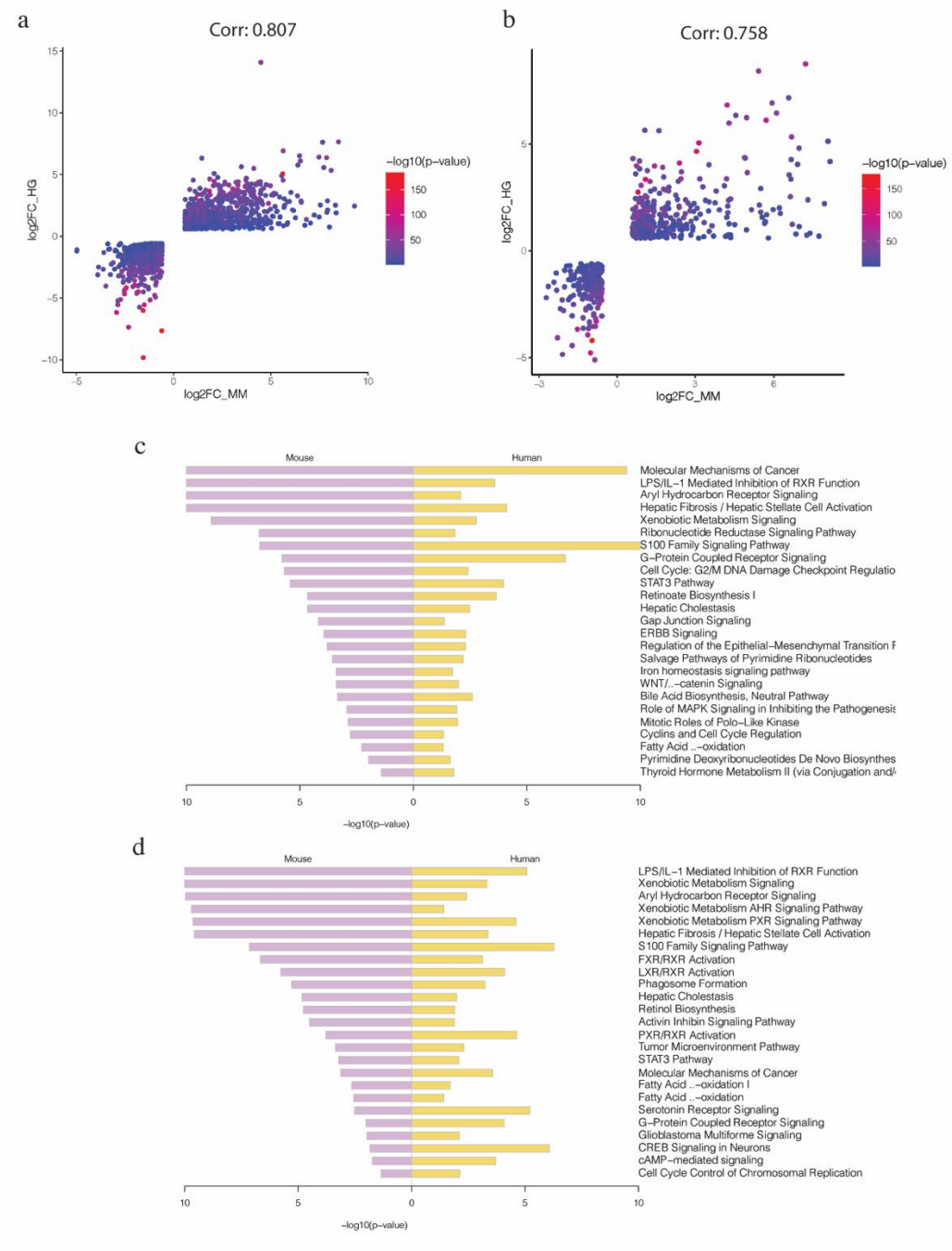
a
Corr: 0.807
log2FC_HG
log2FC_MM
−log10(p−value)
150
100
50
b
Corr: 0.758
log2FC_HG
log2FC_MM
−log10(p−value)
150
100
50
c
Mouse
Human
Molecular Mechanisms of Cancer
LPS/IL−1 Mediated Inhibition of RXR Function
Aryl Hydrocarbon Receptor Signaling
Hepatic Fibrosis / Hepatic Stellate Cell Activation
Xenobiotic Metabolism Signaling
Ribonucleotide Reductase Signaling Pathway
S100 Family Signaling Pathway
G−Protein Coupled Receptor Signaling
Cell Cycle: G2/M DNA Damage Checkpoint Regulatio
STAT3 Pathway
Retinoate Biosynthesis I
Hepatic Cholestasis
Gap Junction Signaling
ERBB Signaling
Regulation of the Epithelial−Mesenchymal Transition F
Salvage Pathways of Pyrimidine Ribonucleotides
Iron homeostasis signaling pathway
WNT/..−catenin Signaling
Bile Acid Biosynthesis, Neutral Pathway
Role of MAPK Signaling in Inhibiting the Pathogenesis
Mitotic Roles of Polo−Like Kinase
Cyclins and Cell Cycle Regulation
Fatty Acid ..−oxidation
Pyrimidine Deoxyribonucleotides De Novo Biosynthes
Thyroid Hormone Metabolism II (via Conjugation and/
−log10(p−value)
d
Mouse
Human
LPS/IL−1 Mediated Inhibition of RXR Function
Xenobiotic Metabolism Signaling
Aryl Hydrocarbon Receptor Signaling
Xenobiotic Metabolism AHR Signaling Pathway
Xenobiotic Metabolism PXR Signaling Pathway
Hepatic Fibrosis / Hepatic Stellate Cell Activation
S100 Family Signaling Pathway
FXR/RXR Activation
LXR/RXR Activation
Phagosome Formation
Hepatic Cholestasis
Retinol Biosynthesis
Activin Inhibin Signaling Pathway
PXR/RXR Activation
Tumor Microenvironment Pathway
STAT3 Pathway
Molecular Mechanisms of Cancer
Fatty Acid ..−oxidation I
Fatty Acid ..−oxidation
Serotonin Receptor Signaling
G−Protein Coupled Receptor Signaling
Glioblastoma Multiforme Signaling
CREB Signaling in Neurons
cAMP−mediated signaling
Cell Cycle Control of Chromosomal Replication
−log10(p−value)

Fig. S7: Comparison of preclinical HCC to clinical HCC with either CTNNB1 mutations and NRF2/MET activation, or NRF2/MET activation alone. (A) Differentially expressed genes show overlap in preclinical HCC model (β-N-M) and HCC subset with similar molecular perturbations, with high correlation (r=0.807 by Pearson's correlation test). (B) Differentially expressed genes show overlap in preclinical HCC model (N-M) and HCC subset with similar molecular perturbations, with high correlation (r=0.758 by Pearson's correlation test). For A-B, Mouse gene expression is plotted on x-axis (MM) and human on y-axis (HG). (C) Plot of top common IPA pathways based on p-value between mouse β-N-M and human HCC similar molecular perturbations. (D) Plot of top common IPA pathways based on p-value between mouse N-M and human HCC similar molecular perturbations.

Fig. S8

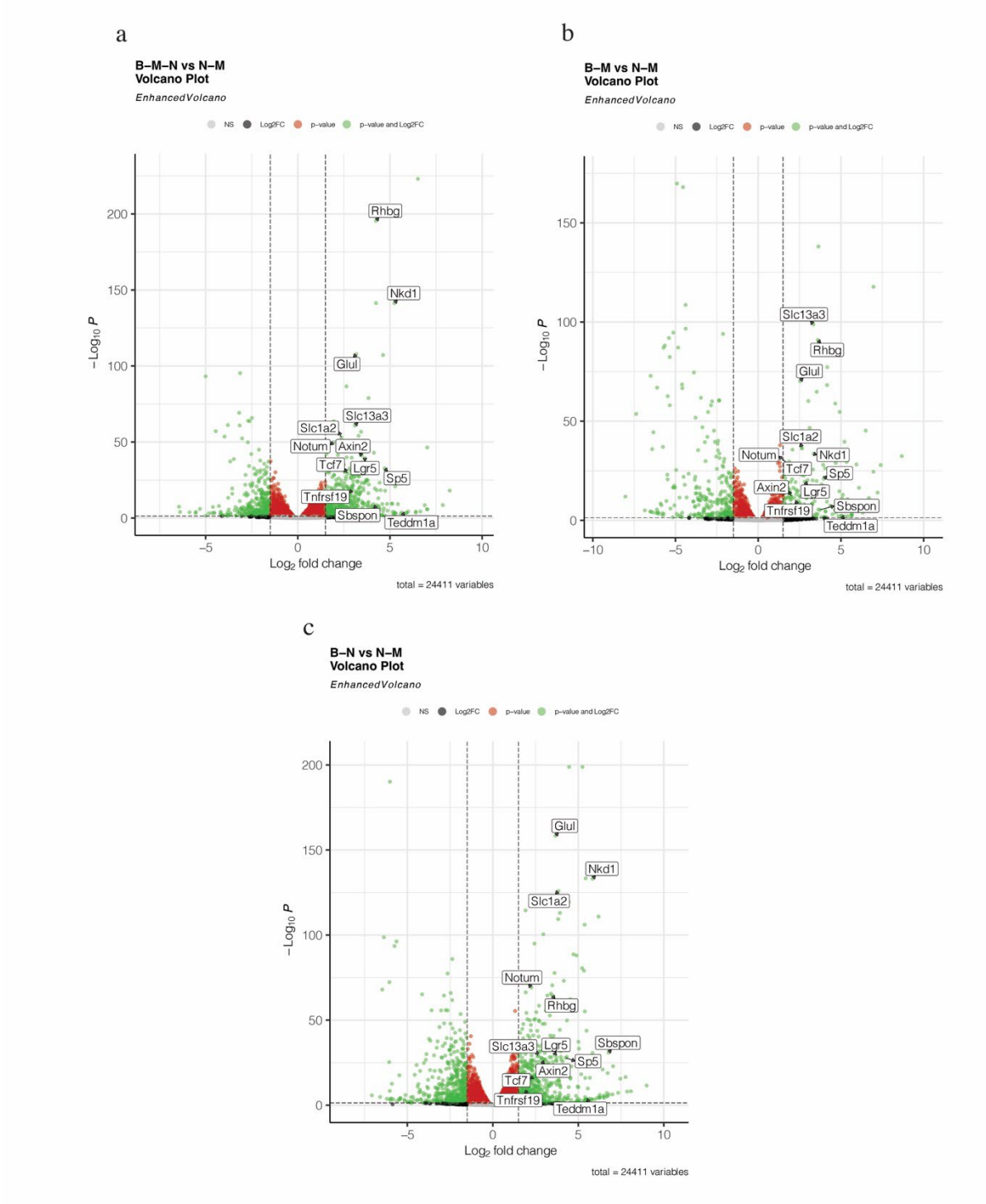
a
B–M–N vs N–M
Volcano Plot
EnhancedVolcano
NS Log2FC p-value p-value and Log2FC
Rhbg
Nkd1
Glul
Slc13a3
Slc1a2
Notum
Axin2
Tcf7
Lgr5
Sp5
Tnfrsf19
Sbspon
Teddm1a
−Log10 P
Log2 fold change
total = 24411 variables
b
B–M vs N–M
Volcano Plot
EnhancedVolcano
NS Log2FC p-value p-value and Log2FC
Slc13a3
Rhbg
Glul
Slc1a2
Notum
Nkd1
Tcf7
Sp5
Axin2
Lgr5
Tnfrsf19
Sbspon
Teddm1a
−Log10 P
Log2 fold change
total = 24411 variables
c
B–N vs N–M
Volcano Plot
EnhancedVolcano
NS Log2FC p-value p-value and Log2FC
Glul
Nkd1
Slc1a2
Notum
Rhbg
Slc13a3
Lgr5
Sbspon
Sp5
Axin2
Tcf7
Tnfrsf19
Teddm1a
−Log10 P
Log2 fold change
total = 24411 variables

Fig. S8: Differential gene expression analysis comparing each β-catenin-mutated tumor model to β-catenin-non-mutated tumor model. (A) Volcano plot showing differential gene expression and enrichment of mutated β-catenin gene signature (MBGS) in β-N-M vs N-M. (B) Volcano plot showing differential gene expression and enrichment of MBGS in β-M vs N-M. (C) Volcano plot showing differential gene expression and enrichment of MBGS in β-N vs N-M. Volcano plot shown are showing differentially expressed genes based on cutoff of absolute log fold change > 1.5 and adjusted $p<0.05$.

Fig. S9


a
Top 25 Pathways
Based on −Log(P−value)
Kinetochore Metaphase Signaling Pathway
FXR/RXR Activation
LPS/IL−1 Mediated Inhibition of RXR Function
Estrogen Biosynthesis
Cell Cycle Control of Chromosomal Replication
LXR/RXR Activation
Mitotic Roles of Polo−Like Kinase
Coagulation System
Pathogen Induced Cytokine Storm Signaling Pathway
Oxidative Ethanol Degradation III
Complement System
Superpathway of Melatonin Degradation
Superpathway of Citrulline Metabolism
S100 Family Signaling Pathway
Bupropion Degradation
Androgen Biosynthesis
DHCR24 Signaling Pathway
Pulmonary Fibrosis Idiopathic Signaling Pathway
Pulmonary Healing Signaling Pathway
Aryl Hydrocarbon Receptor Signaling
Melatonin Degradation I
Citrulline Biosynthesis
Histidine Degradation VI
Acetone Degradation I (to Methylglyoxal)
Urea Cycle
Pathways
Z−Score
4
2
0
−2
0
5
10
15
20
−log(p−value)
b
Top 25 Pathways
Based on −Log(P−value)
LPS/IL−1 Mediated Inhibition of RXR Function
Xenobiotic Metabolism CAR Signaling Pathway
Xenobiotic Metabolism AHR Signaling Pathway
Aryl Hydrocarbon Receptor Signaling
Xenobiotic Metabolism Signaling
Xenobiotic Metabolism PXR Signaling Pathway
NRF2−mediated Oxidative Stress Response
Estrogen Biosynthesis
Acetone Degradation I (to Methylglyoxal)
Oxidative Ethanol Degradation III
Glutathione−mediated Detoxification
Nicotine Degradation II
S100 Family Signaling Pathway
Nicotine Degradation III
Melatonin Degradation I
Bupropion Degradation
PXR/RXR Activation
Role of JAK family kinases in IL−6−type Cytokine Signaling
Superpathway of Melatonin Degradation
Androgen Biosynthesis
Glutaminergic Receptor Signaling Pathway (Enhanced)
Hepatic Fibrosis / Hepatic Stellate Cell Activation
CREB Signaling in Neurons
Gustation Pathway
Glutathione Redox Reactions I
Pathways
Z−Score
1
0
−1
−2
−3
0
3
6
9
−log(p−value)
c
Top 25 Pathways
Based on −Log(P−value)
Kinetochore Metaphase Signaling Pathway
LPS/IL−1 Mediated Inhibition of RXR Function
FXR/RXR Activation
Acute Phase Response Signaling
LXR/RXR Activation
Pathogen Induced Cytokine Storm Signaling Pathway
Coagulation System
Oxidative Ethanol Degradation III
Hepatic Fibrosis / Hepatic Stellate Cell Activation
Aryl Hydrocarbon Receptor Signaling
Xenobiotic Metabolism PXR Signaling Pathway
Cell Cycle Control of Chromosomal Replication
Xenobiotic Metabolism Signaling
Triacylglycerol Degradation
Androgen Biosynthesis
PXR/RXR Activation
NRF2−mediated Oxidative Stress Response
Xenobiotic Metabolism CAR Signaling Pathway
Histidine Degradation VI
Estrogen Biosynthesis
Mitotic Roles of Polo−Like Kinase
DHCR24 Signaling Pathway
Histidine Degradation III
Heparan Sulfate Biosynthesis (Late Stages)
Complement System
Pathways
Z−Score
4
2
0
−2
0
5
10
15
20
−log(p−value)

Fig. S9: Pathway analysis comparing each β-catenin-mutated tumor model to β-catenin-non-mutated tumor model. (A) Bar plot showing IPA analysis (top 25 pathways based on p-value) on differentially expressed genes comparing β-N-M vs N-M. (B) Bar plot showing IPA analysis (top 25 pathways based on p-value) on differentially expressed genes comparing β-M vs N-M. (C) Bar plot showing IPA analysis (top 25 pathways based on p-value) on differentially expressed genes comparing β-N vs N-M. IPA analysis was performed based on genes with FDR=0.05 and absolute log fold change > 1.5.

Fig. S10

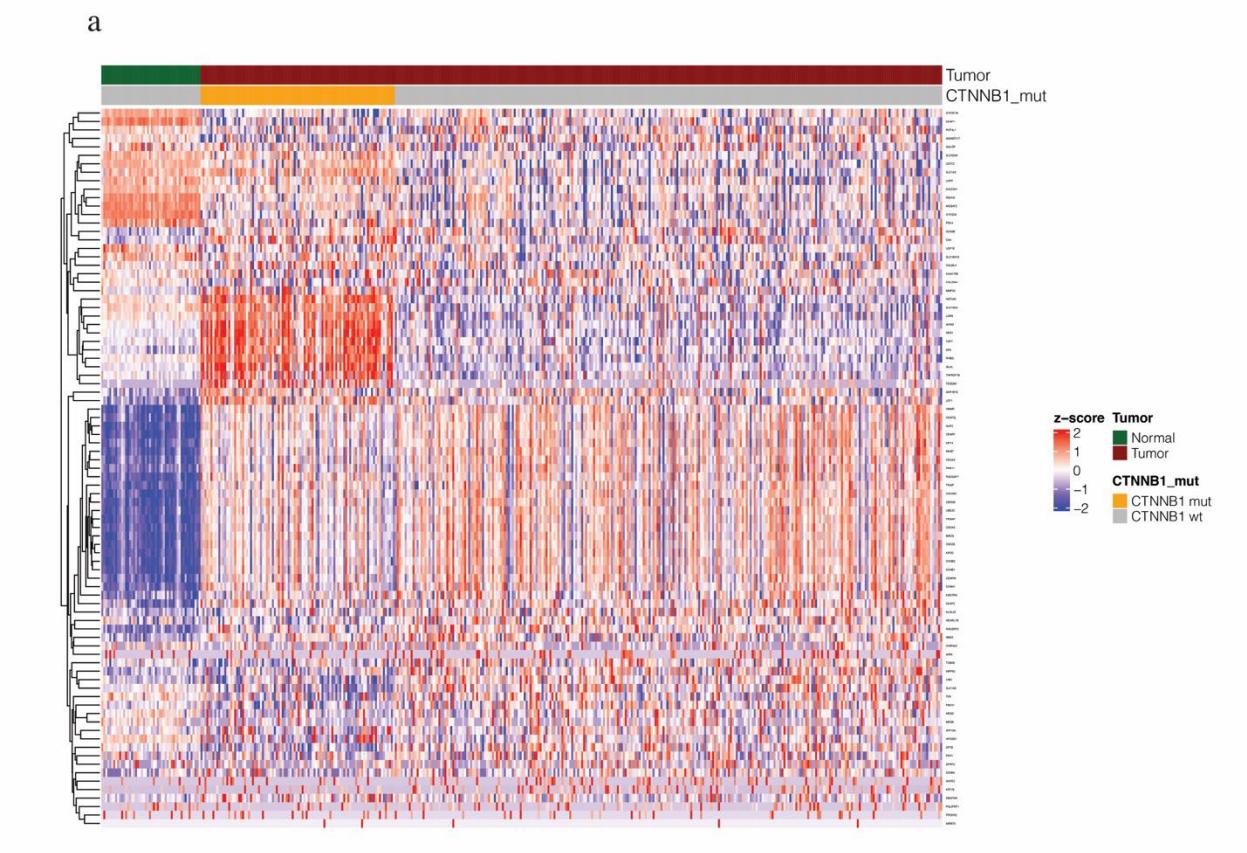
a
Tumor
CTNNB1_mut
z−score
2
1
0
−1
−2
Tumor
Normal
Tumor
CTNNB1_mut
CTNNB1 mut
CTNNB1 wt

Fig. S10: Visualization in TCGA-LIHC of 85 human ortholog genes of the 95 murine genes that were enriched in β-catenin-mutated tumors. Heatmap of 374 TCGA-LIHC HCC cases and 50 adjacent normal cases for the 85 mapped human orthologs of the 95 differentially expressed mouse genes. Normalized and scaled gene expression based on z-score is shown.

Fig. S11

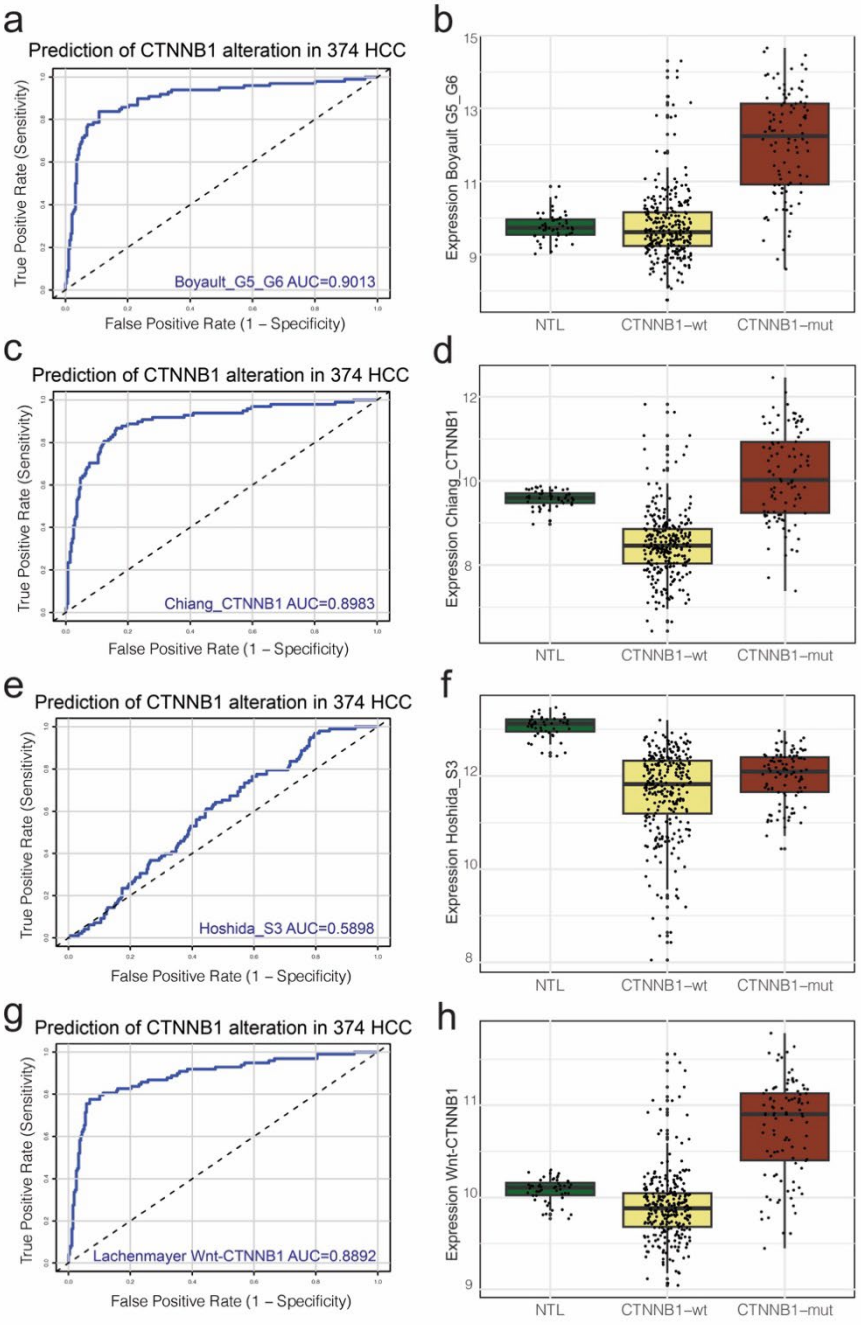
a
Prediction of CTNNB1 alteration in 374 HCC
True Positive Rate (Sensitivity)
False Positive Rate (1 – Specificity)
Boyault_G5_G6 AUC=0.9013
b
Expression Boyault G5_G6
NTL
CTNNB1–wt
CTNNB1–mut
c
Prediction of CTNNB1 alteration in 374 HCC
True Positive Rate (Sensitivity)
False Positive Rate (1 – Specificity)
Chiang_CTNNB1 AUC=0.8983
d
Expression Chiang_CTNNB1
NTL
CTNNB1–wt
CTNNB1–mut
e
Prediction of CTNNB1 alteration in 374 HCC
True Positive Rate (Sensitivity)
False Positive Rate (1 – Specificity)
Hoshida_S3 AUC=0.5898
f
Expression Hoshida_S3
NTL
CTNNB1–wt
CTNNB1–mut
g
Prediction of CTNNB1 alteration in 374 HCC
True Positive Rate (Sensitivity)
False Positive Rate (1 – Specificity)
Lachenmayer Wnt-CTNNB1 AUC=0.8892
h
Expression Wnt-CTNNB1
NTL
CTNNB1–wt
CTNNB1–mut

Fig. S11. Ability of previously published molecular subclass signatures to predict CTNNB1 mutational status in TCGA-LIHC dataset. ROC AUC and composite average normalized expression value of the gene signature scores for Boyault G5/G6 (a-b), Chiang CTNNB1 (c-d), Hoshida S3 (e-f), and Lachenmayer Wnt-CTNNB1 (g-h). The TCGA-LIHC cohort has CTNNB1-mutated (n=98), CTNNB1-wild-type (n=276), and normal tumor liver (n=50) samples. For (B), (D), (F), (H), Individual values per patient are depicted with bold line in middle representing the median and outside boxes showing inner quartile ranges. One-way ANOVA p-value for (B) is ***p<2.22e-16. One-way ANOVA p-value for (D) is ***p<2.22e-16. One-way ANOVA p-value for (F) is ***p<2.22e-16. One-way ANOVA p-value for (H) is ***p<2.22e-16. Levels of significance: *p<0.05, **p<0.001, ***p<0.0001.

Fig. S12

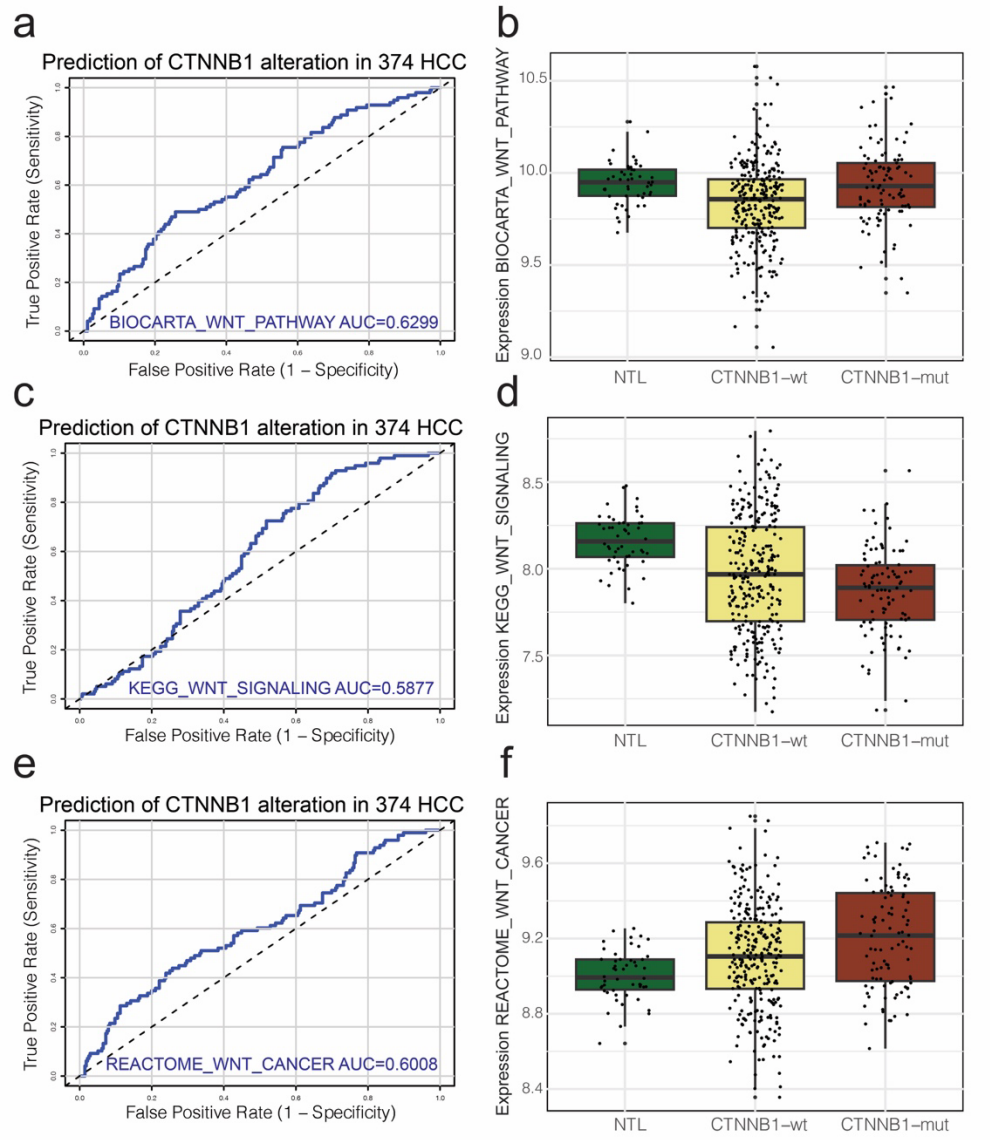
a
Prediction of CTNNB1 alteration in 374 HCC
True Positive Rate (Sensitivity)
False Positive Rate (1 – Specificity)
BIOCARTA_WNT_PATHWAY AUC=0.6299
b
Expression BIOCARTA_WNT_PATHWAY
10.5
10.0
9.5
9.0
NTL
CTNNB1–wt
CTNNB1–mut
c
Prediction of CTNNB1 alteration in 374 HCC
True Positive Rate (Sensitivity)
False Positive Rate (1 – Specificity)
KEGG_WNT_SIGNALING AUC=0.5877
d
Expression KEGG_WNT_SIGNALING
8.5
8.0
7.5
NTL
CTNNB1–wt
CTNNB1–mut
e
Prediction of CTNNB1 alteration in 374 HCC
True Positive Rate (Sensitivity)
False Positive Rate (1 – Specificity)
REACTOME_WNT_CANCER AUC=0.6008
f
Expression REACTOME_WNT_CANCER
9.6
9.2
8.8
8.4
NTL
CTNNB1–wt
CTNNB1–mut

Fig. S12. Ability of previously published Wnt signatures to predict CTNNB1 mutational status in TCGA-LIHC dataset. ROC AUC and composite average normalized expression values for each of the different gene signatures specifically for the BIOCARTA_WNT_PATHWAY (a-b), KEGG_WNT_SIGNALING_PATHWAY (c-d), and REACTOME_SIGNALING_BY_WNT_IN_CANCER (e-f) signatures. The TCGA-LIHC cohort has CTNNB1-mutated (n=98), CTNNB1-wild-type (n=276), and normal tumor liver (n=50) samples. For (B), (D), (F), Individual values per patient are depicted with bold line in middle representing the median and outside boxes showing inner quartile ranges. One-way ANOVA p-value for (B) is ***p<1.23e-5. One-way ANOVA p-value for (D) is ***p<3.32e-7. One-way ANOVA p-value for (F) is ***p<2.49e-5. Levels of significance: *p<0.05, **p<0.001, ***p<0.0001.

Fig. S13

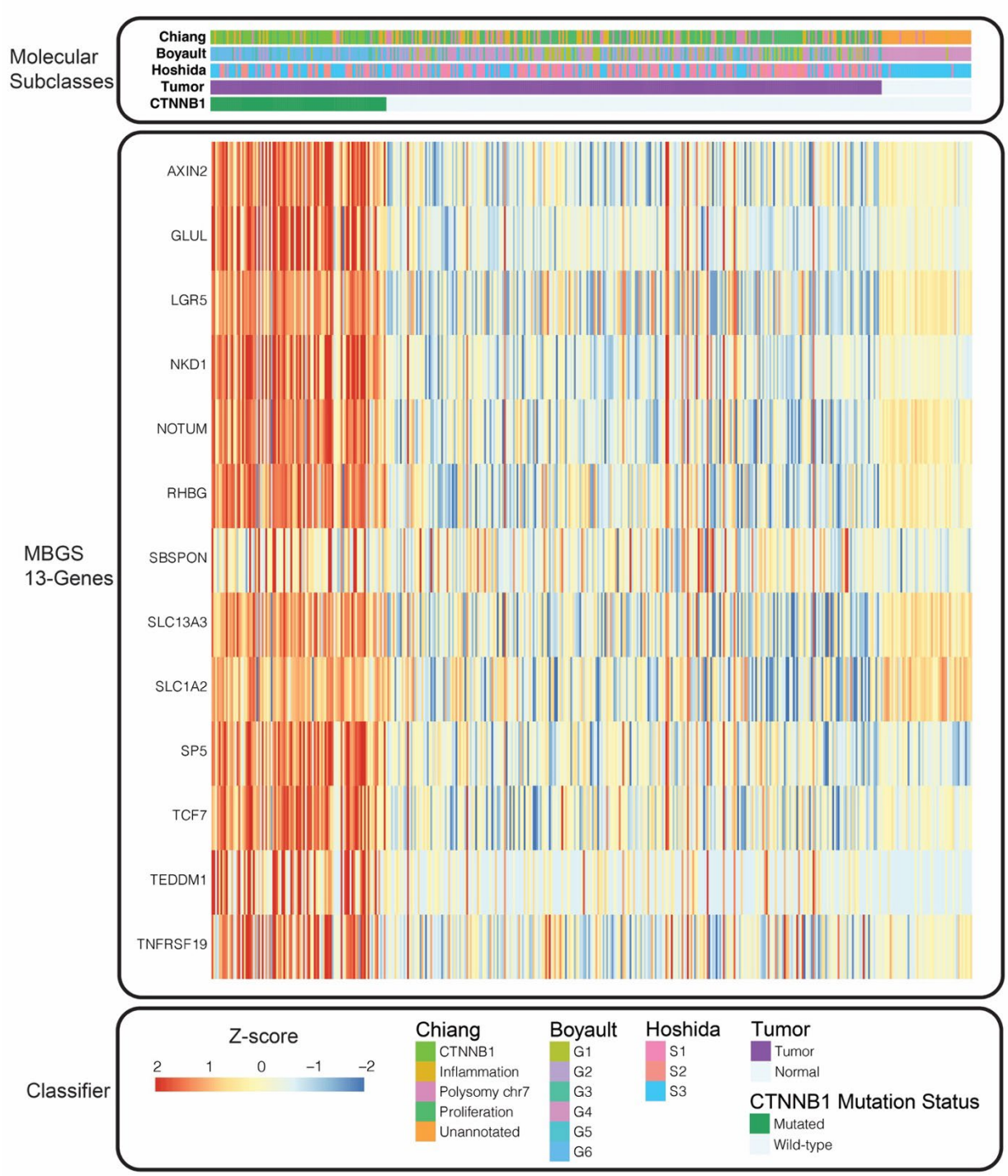
Molecular Subclasses
Chiang
Boyault
Hoshida
Tumor
CTNNB1
MBGS 13-Genes
AXIN2
GLUL
LGR5
NKD1
NOTUM
RHBG
SBSPON
SLC13A3
SLC1A2
SP5
TCF7
TEDDM1
TNFRSF19
Classifier
Z-score
2 1 0 −1 −2
Chiang
CTNNB1
Inflammation
Polysomy chr7
Proliferation
Unannotated
Boyault
G1
G2
G3
G4
G5
G6
Hoshida
S1
S2
S3
Tumor
Tumor
Normal
CTNNB1 Mutation Status
Mutated
Wild-type

Fig. S13. Heatmap overlapping all molecular subclasses, CTNNB1-mutated patients, and MBGS expression depicts MBGS is specific to CTNNB1 mutations. Normalized gene expression scaled based on z-score is shown.

Fig. S14

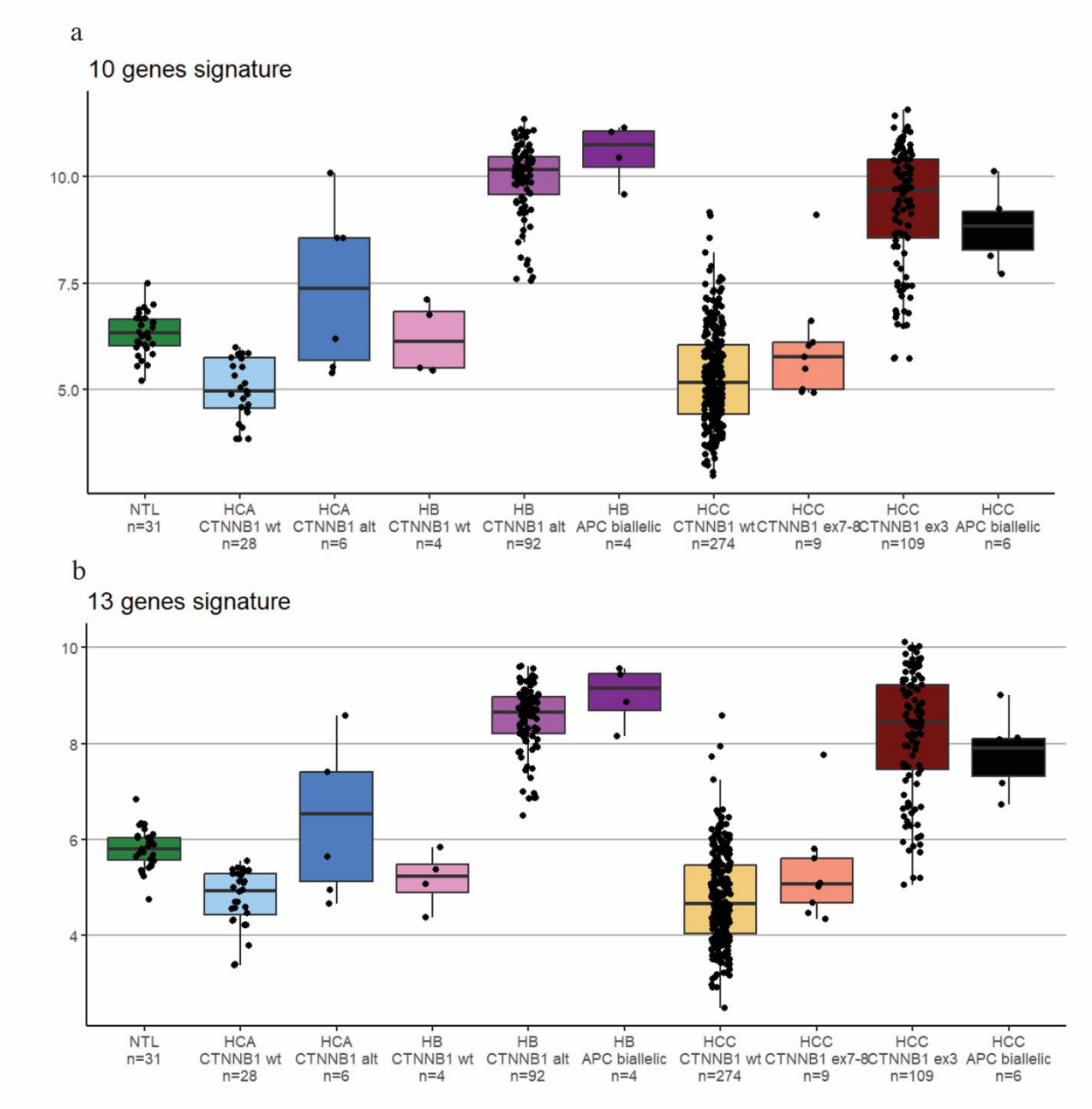
a
10 genes signature
10.0
7.5
5.0
NTL n=31
HCA CTNNB1 wt n=28
HCA CTNNB1 alt n=6
HB CTNNB1 wt n=4
HB CTNNB1 alt n=92
HB APC biallelic n=4
HCC CTNNB1 wt n=274
HCC CTNNB1 ex7-8 n=9
HCC CTNNB1 ex3 n=109
HCC APC biallelic n=6
b
13 genes signature
10
8
6
4
NTL n=31
HCA CTNNB1 wt n=28
HCA CTNNB1 alt n=6
HB CTNNB1 wt n=4
HB CTNNB1 alt n=92
HB APC biallelic n=4
HCC CTNNB1 wt n=274
HCC CTNNB1 ex7-8 n=9
HCC CTNNB1 ex3 n=109
HCC APC biallelic n=6

Fig. S14: MBGS expression across hepatocellular adenoma, hepatoblastoma, and HCC with different exon mutations. (A) Boxplot of 10-gene MBGS in French cohort of hepatocellular adenoma, hepatoblastoma, and HCC with exon 3, exon 7, and APC biallelic mutations. For (A) and (B) Individual values per patient are depicted with bold line in middle representing the median and outside boxes showing inner quartile ranges; no statistical test was used, but depicted this way for visual representation across the different subclasses and to show distribution of values within the different groups.

Fig. S15

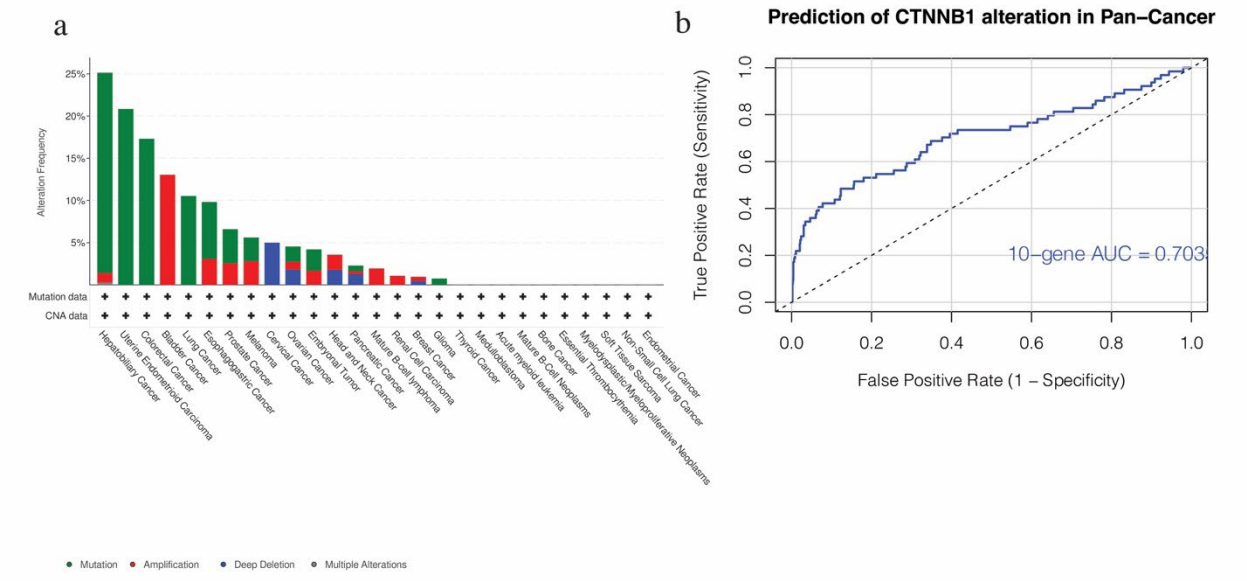
a
Alteration Frequency
25%
20%
15%
10%
5%
Mutation data
CNA data
Hepatobiliary Cancer
Uterine Endometrioid Carcinoma
Colorectal Cancer
Bladder Cancer
Lung Cancer
Esophagogastric Cancer
Prostate Cancer
Melanoma
Cervical Cancer
Ovarian Cancer
Embryonal Tumor
Head and Neck Cancer
Pancreatic Cancer
Mature B-cell lymphoma
Renal Cell Carcinoma
Breast Cancer
Glioma
Thyroid Cancer
Medulloblastoma
Acute myeloid leukemia
Mature B-cell Neoplasms
Bone Cancer
Essential Thrombocythemia
Myelodysplastic/Myeloproliferative Neoplasms
Soft Tissue Sarcoma
Non-Small Cell Lung Cancer
Endometrial Cancer
Mutation
Amplification
Deep Deletion
Multiple Alterations
b
Prediction of CTNNB1 alteration in Pan–Cancer
True Positive Rate (Sensitivity)
0.0
0.2
0.4
0.6
0.8
1.0
10–gene AUC = 0.703
False Positive Rate (1 – Specificity)

Fig. S15: MBGS's predictive ability in pan-cancer atlas. (A) Bar plot of different tumor types with CTNNB1 alteration frequency in ICGC/TCGA cohort with 2,565 patients across 2,683 samples of multiple tumor types, of which 178 samples had CTNNB1 mutations. Image directly from cBioPortal.org website of ICGC/TCGA patient cohort from "Cancer Types Summary" tab following query of CTNNB1 mutational status. (B) AUC/ROC curve for prediction of CTNNB1 mutation in pan-cancer setting with AUC of 0.7035 for 10-gene MBGS.

Fig. S16

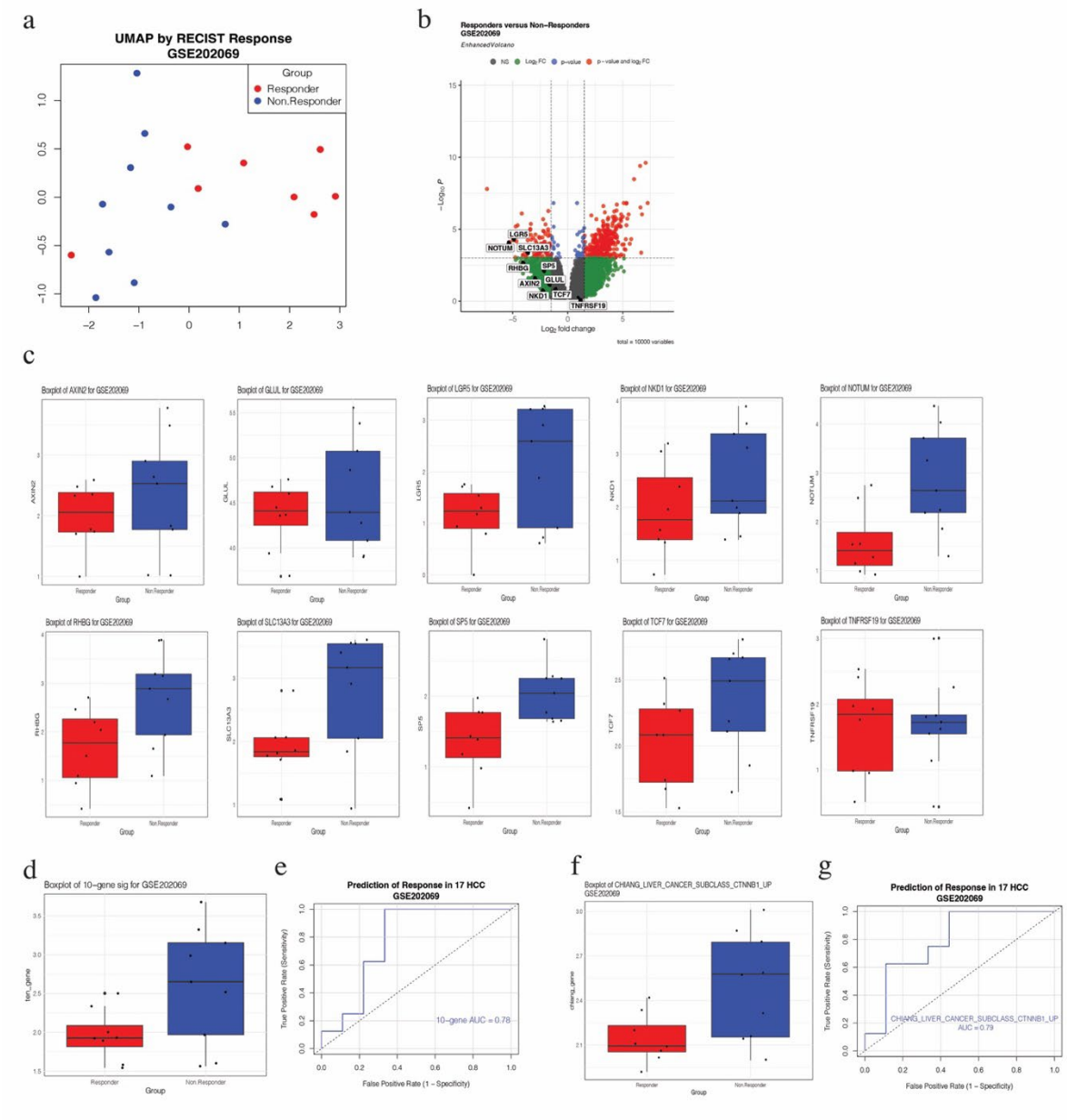
a
UMAP by RECIST Response
GSE202069
Group
Responder
Non.Responder
b
Responders versus Non-Responders
GSE202069
EnhancedVolcano
LGR5
NOTUM
SLC13A3
RHBG
SP5
AXIN2
GLUL
NKD1
TCF7
TNFRSF19
Log2 fold change
c
Boxplot of AXIN2 for GSE202069
Boxplot of GLUL for GSE202069
Boxplot of LGR5 for GSE202069
Boxplot of NKD1 for GSE202069
Boxplot of NOTUM for GSE202069
Boxplot of RHBG for GSE202069
Boxplot of SLC13A3 for GSE202069
Boxplot of SP5 for GSE202069
Boxplot of TCF7 for GSE202069
Boxplot of TNFRSF19 for GSE202069
Responder
Non.Responder
Group
d
Boxplot of 10−gene sig for GSE202069
tan_gene
e
Prediction of Response in 17 HCC
GSE202069
10−gene AUC = 0.78
True Positive Rate (Sensitivity)
False Positive Rate (1 − Specificity)
f
Boxplot of CHIANG_LIVER_CANCER_SUBCLASS_CTNNB1_UP
GSE202069
chiang_gene
g
Prediction of Response in 17 HCC
GSE202069
CHIANG_LIVER_CANCER_SUBCLASS_CTNNB1_UP
AUC = 0.79

Fig. S16: MBGS expression in small HCC immunotherapy cohort. (A) UMAP of responders and non-responders in GSE202069 demonstrating separation of responders and non-responders in terms of gene expression (n=8 responders and n=9 non-responders). (B) Volcano plot of differentially expressed genes comparing responders and non-responders demonstrating enrichment of MBGS in downregulated genes in responders based on differential gene expression with cutoff of p<1e-3 and absolute log fold change > 1.5. (C) Boxplots of all 10 genes in 10-gene MBGS stratified by responders and non-responders in GSE202069. Welch two-sample t-test p-value comparing responders versus non-responder patients for AXIN2 (p=0.3979), GLUL (p=0.3356), LGR5 (*p=0.0384), NKD1 (p=0.2118), NOTUM (*p=0.01031), RHBG (*p=0.03007), SLC13A3 (*p=0.0297), SP5 (*p=0.009038), TCF7 (p=0.1019), TNFRSF19 (p=0.8363). (D) Boxplot comparing expression of 10-gene MBGS in responders and non-responders. Welch two-sample t-test p-value comparing responders versus non-responder patients is *p=0.04176. (E) AUC/ROC curve demonstrating AUC of 0.78 using 10-gene MBGS to classify immunotherapy resistance in this cohort. (F) Boxplot comparing expression of CHIANG_LIVER_CANCER_SUBCLASS_CTNNB1_UP gene signature in responders and non-responders. Welch two-sample t-test p-value comparing responders versus non-responder patients is *p=0.02256. (G) AUC/ROC curve demonstrating AUC of 0.79 using CHIANG_LIVER_CANCER_SUBCLASS_CTNNB1_UP gene signature to classify immunotherapy resistance in this cohort. All boxplots show individual values per patient depicted with bold line in middle representing the median and outside boxes showing inner quartile ranges. Levels of significance: *p<0.05, **p<0.001, ***p<0.0001.

Fig. S17

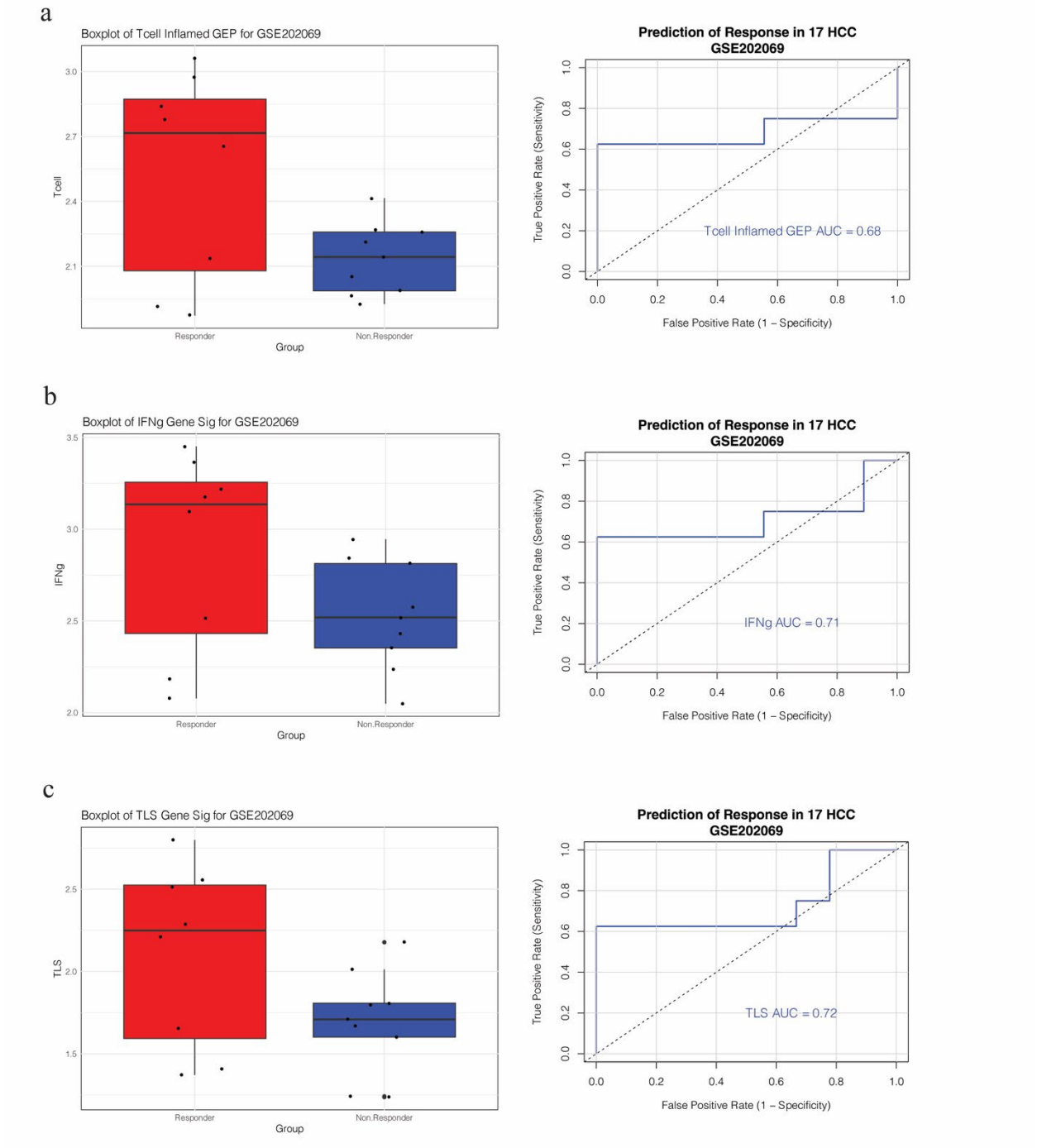
a
Boxplot of Tcell Inflamed GEP for GSE202069
Tcell
Responder
Non.Responder
Group
Prediction of Response in 17 HCC GSE202069
True Positive Rate (Sensitivity)
False Positive Rate (1 – Specificity)
Tcell Inflamed GEP AUC = 0.68
b
Boxplot of IFNg Gene Sig for GSE202069
IFNg
Responder
Non.Responder
Group
Prediction of Response in 17 HCC GSE202069
True Positive Rate (Sensitivity)
False Positive Rate (1 – Specificity)
IFNg AUC = 0.71
c
Boxplot of TLS Gene Sig for GSE202069
TLS
Responder
Non.Responder
Group
Prediction of Response in 17 HCC GSE202069
True Positive Rate (Sensitivity)
False Positive Rate (1 – Specificity)
TLS AUC = 0.72

Fig. S17: Prediction of immunotherapy resistance using previously published gene signatures in small HCC immunotherapy cohort. (A) T cell-inflamed gene expression profile, (B) IFNg response signature, and (C) tertiary lymphoid structure (TLS) signature Boxplots and AUC/ROC curves for GSE202069 to predict immunotherapy resistance (ROC AUC: 0.68, 0.71, 0.72, respectively). Welch two-sample t-test p-value comparing responders versus non-responder patients for T-cell inflamed GEP (p=0.05761), IFNg response signature (p=0.1294), and TLS signature (p=0.0943). All boxplots show individual values per patient depicted with bold line in middle representing the median and outside boxes showing inner quartile ranges. Levels of significance: *p<0.05, **p<0.001, ***p<0.0001.

Fig. S18

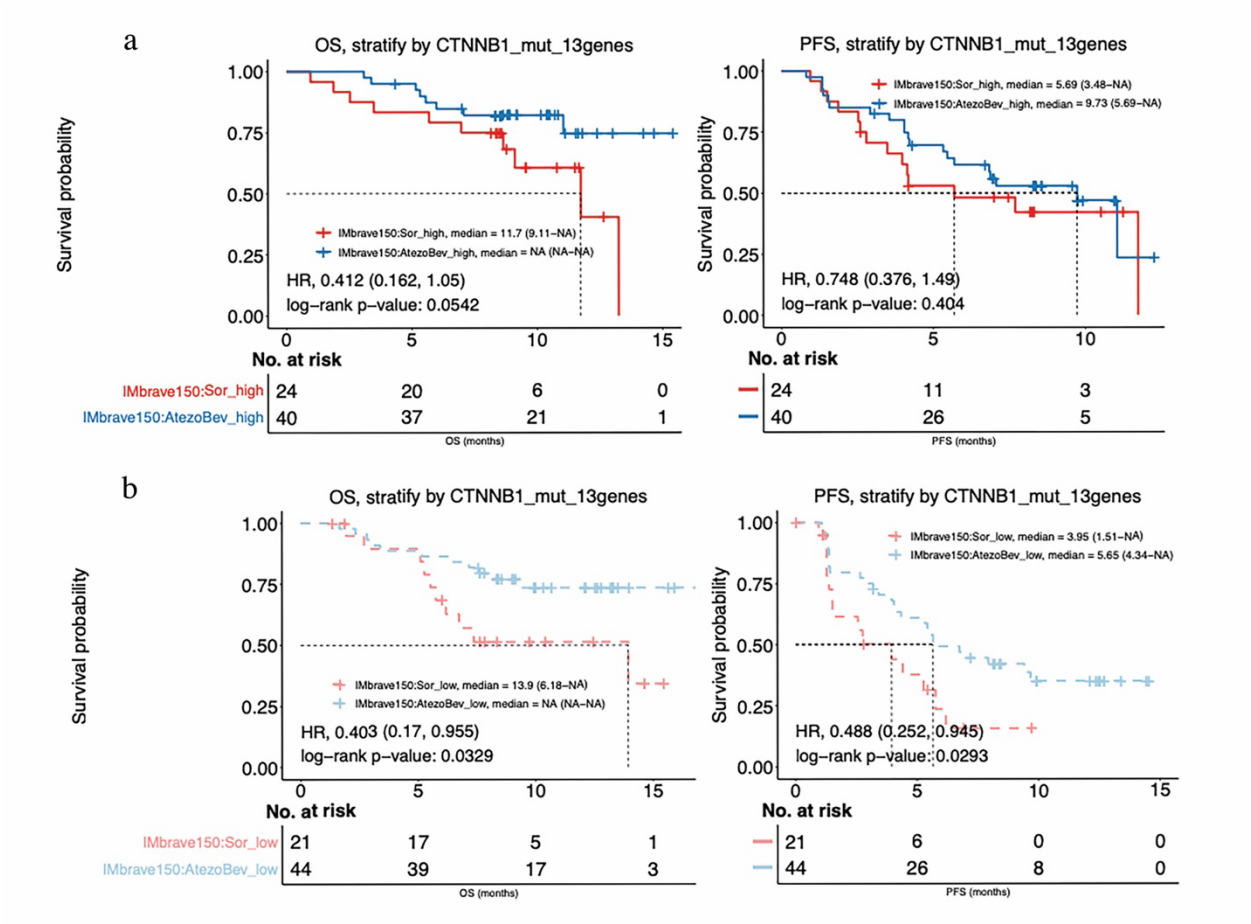
a
OS, stratify by CTNNB1_mut_13genes
Survival probability
1.00
0.75
0.50
0.25
0.00
IMbrave150:Sor_high, median = 11.7 (9.11–NA)
IMbrave150:AtezoBev_high, median = NA (NA–NA)
HR, 0.412 (0.162, 1.05)
log–rank p–value: 0.0542
0 5 10 15
No. at risk
IMbrave150:Sor_high 24 20 6 0
IMbrave150:AtezoBev_high 40 37 21 1
OS (months)
PFS, stratify by CTNNB1_mut_13genes
IMbrave150:Sor_high, median = 5.69 (3.48–NA)
IMbrave150:AtezoBev_high, median = 9.73 (5.69–NA)
HR, 0.748 (0.376, 1.49)
log–rank p–value: 0.404
0 5 10
No. at risk
24 11 3
40 26 5
PFS (months)
b
OS, stratify by CTNNB1_mut_13genes
IMbrave150:Sor_low, median = 13.9 (6.18–NA)
IMbrave150:AtezoBev_low, median = NA (NA–NA)
HR, 0.403 (0.17, 0.955)
log–rank p–value: 0.0329
No. at risk
IMbrave150:Sor_low 21 17 5 1
IMbrave150:AtezoBev_low 44 39 17 3
OS (months)
PFS, stratify by CTNNB1_mut_13genes
IMbrave150:Sor_low, median = 3.95 (1.51–NA)
IMbrave150:AtezoBev_low, median = 5.65 (4.34–NA)
HR, 0.488 (0.252, 0.945)
log–rank p–value: 0.0293
No. at risk
21 6 0 0
44 26 8 0
PFS (months)

Fig. S18. High MBGS expression is associated with response to sorafenib. (A) MBGS high patients had limited overall (left) and progression-free survival (right) (OS/PFS) benefit comparing treatment groups. Log-rank p-value for OS is p= 0.0542. Log-rank p-value for OS is p= 0.404. (B) MBGS low patients had improved OS and PFS on atezolizumab/bevacizumab versus sorafenib. Log-rank p-value for OS is *p= 0.0329. Log-rank p-value for OS is *p= 0.0293. MBGS high/low was determined based on median expression value. Log-rank test was used to determine differences in mean survival time. The Kaplan-Meier curves shown here for (A) and (B) are split apart from the Kaplan-Meier curves shown in **Fig. 7d-e** to illustrate the specific differences between indicated expression groups and treatment arms. Levels of significance: *p<0.05, **p<0.001, ***p<0.0001.

Fig. S19

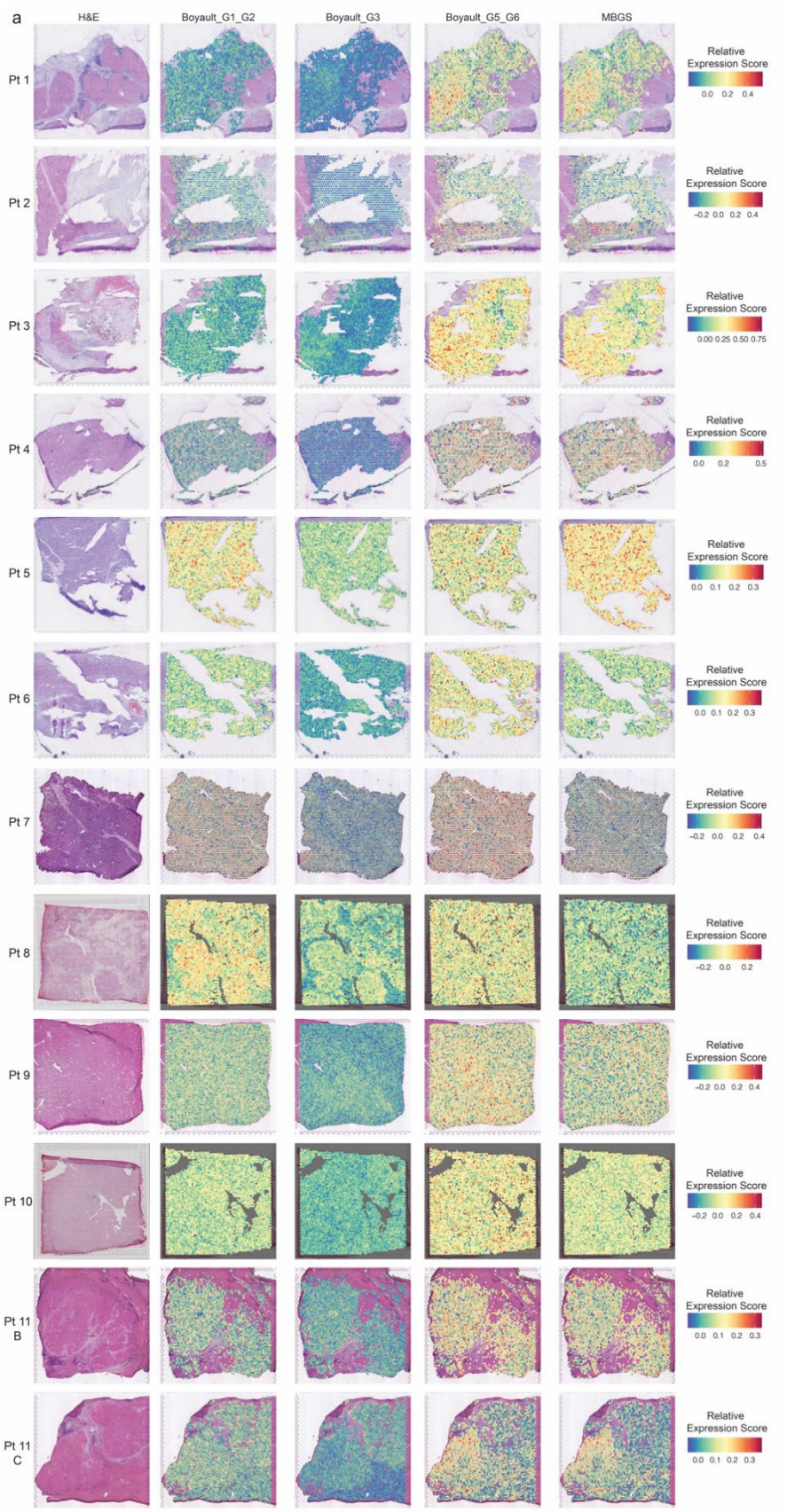
a
H&E
Boyault_G1_G2
Boyault_G3
Boyault_G5_G6
MBGS
Pt 1
Pt 2
Pt 3
Pt 4
Pt 5
Pt 6
Pt 7
Pt 8
Pt 9
Pt 10
Pt 11 B
Pt 11 C
Relative Expression Score
0.0 0.2 0.4
−0.2 0.0 0.2 0.4
0.00 0.25 0.50 0.75
0.0 0.2 0.5
0.0 0.1 0.2 0.3
−0.2 0.0 0.2

Fig. S19. Expression of Boyault molecular subclassification onto spatial transcriptomic tissue section compared to MBGS. 11 (12 total slides) individual patient slides with H&E are shown with expression of various subclassification gene signatures shown with each spot. All the slides are normalized to the same expression scale. Relative expression module scores are depicted with red being higher expression and blue being lower expression. Pt 1 and Pt 8 slides are shown in **Fig. 8a**, but are depicted also here again to show as part of the total cohort analyzed.

Fig. S20

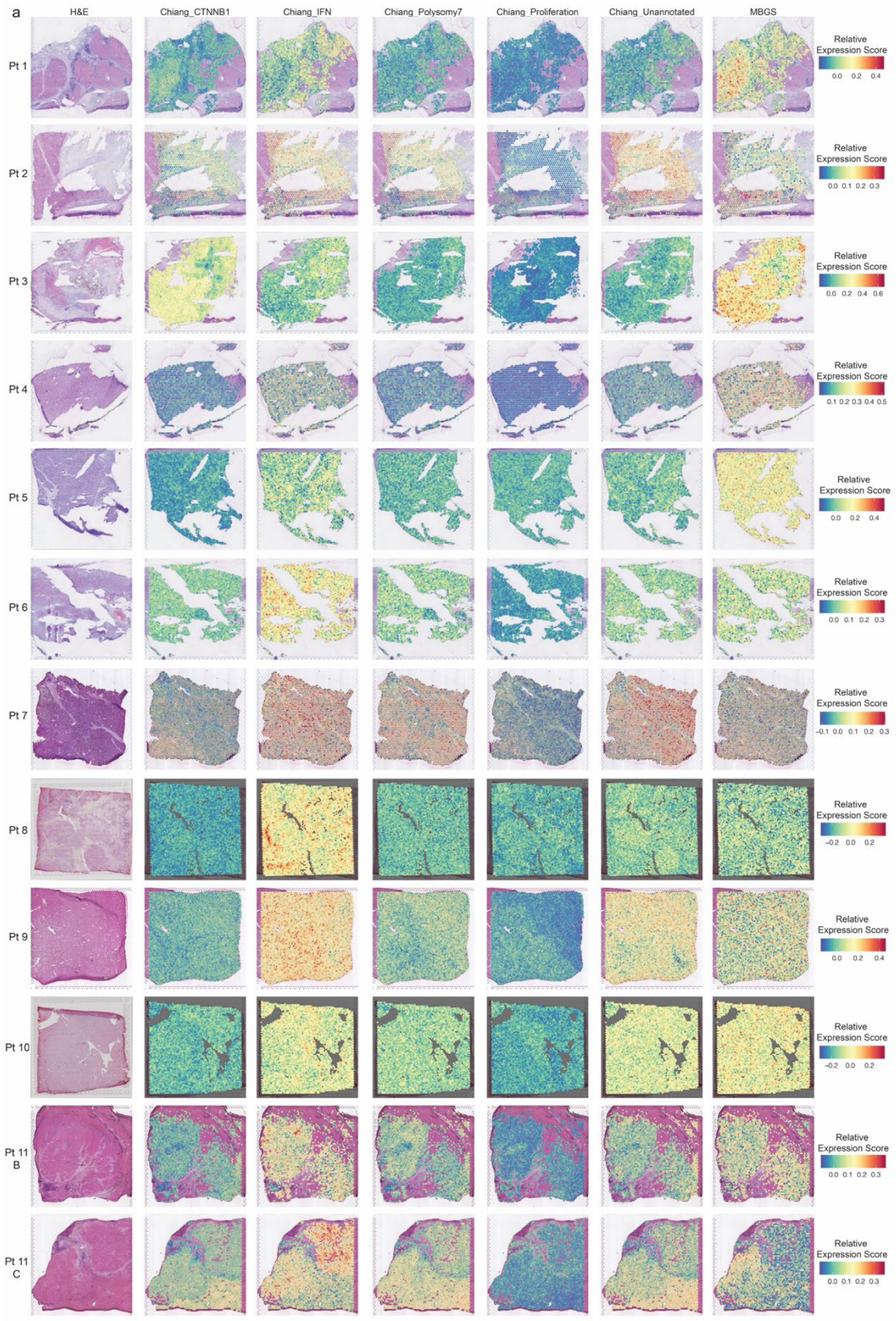
a
H&E
Chiang_CTNNB1
Chiang_IFN
Chiang_Polysomy7
Chiang_Proliferation
Chiang_Unannotated
MBGS
Pt 1
Pt 2
Pt 3
Pt 4
Pt 5
Pt 6
Pt 7
Pt 8
Pt 9
Pt 10
Pt 11 B
Pt 11 C
Relative Expression Score

Fig. S20. Expression of Chiang molecular subclassification onto spatial transcriptomic tissue section compared to MBGS. 11 (12 total slides) patient slides with H&E are shown with expression of various subclassification gene signatures shown with each spot. All the slides are normalized to the same expression scale. Relative expression module scores are depicted with red being higher expression and blue being lower expression.

Fig. S21

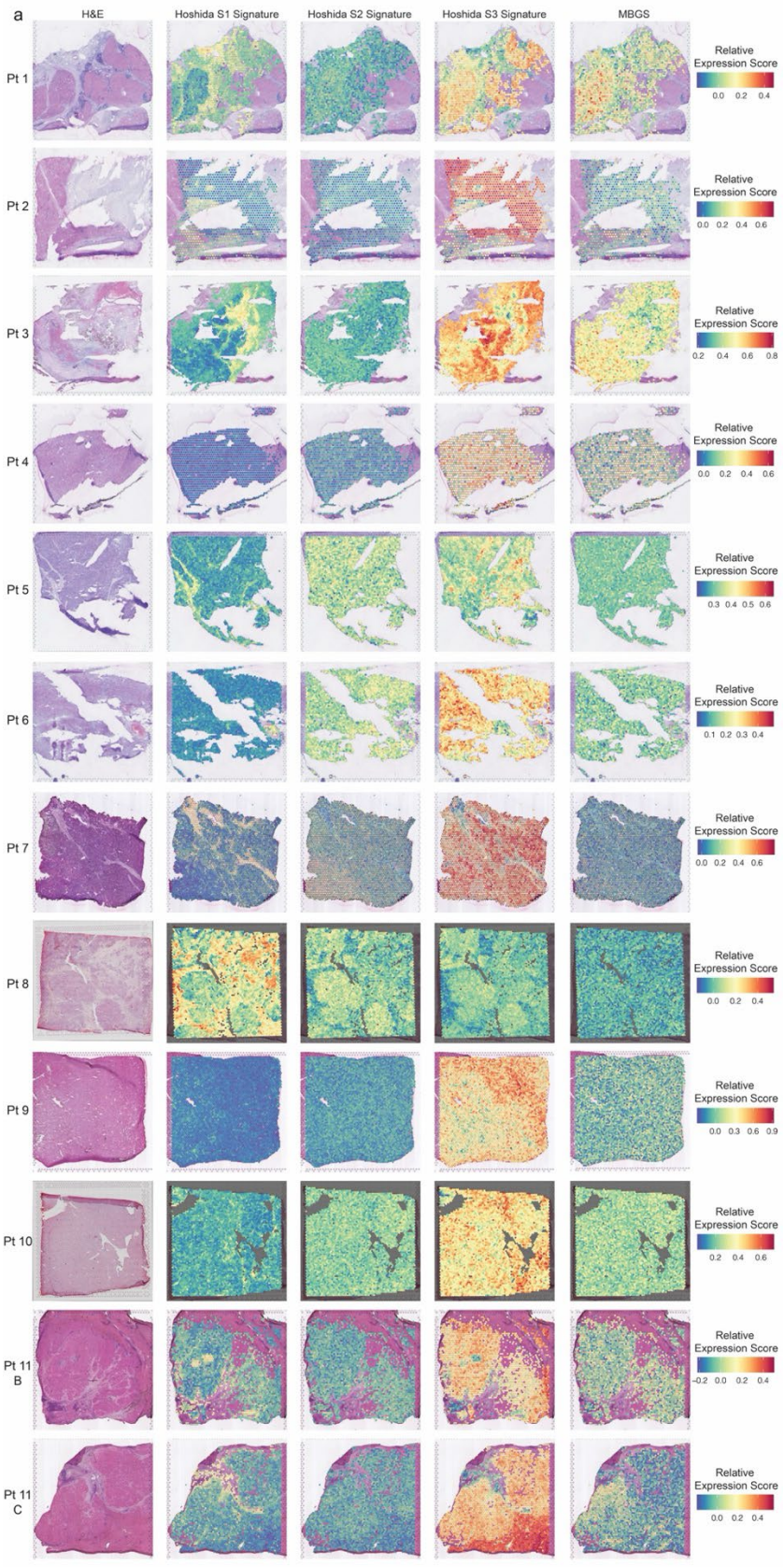
a
H&E
Hoshida S1 Signature
Hoshida S2 Signature
Hoshida S3 Signature
MBGS
Pt 1
Pt 2
Pt 3
Pt 4
Pt 5
Pt 6
Pt 7
Pt 8
Pt 9
Pt 10
Pt 11 B
Pt 11 C
Relative Expression Score
0.0 0.2 0.4
0.0 0.2 0.4 0.6
0.2 0.4 0.6 0.8
0.0 0.2 0.4 0.6
0.3 0.4 0.5 0.6
0.1 0.2 0.3 0.4
0.0 0.2 0.4 0.6
0.0 0.2 0.4
0.0 0.3 0.6 0.9
0.2 0.4 0.6
-0.2 0.0 0.2 0.4
0.0 0.2 0.4

Fig. S21. Expression of Hoshida molecular subclassification onto spatial transcriptomic tissue section compared to MBGS. 11 (12 total slides) patient slides with H&E are shown with expression of various subclassification gene signatures shown with each spot. All the slides are normalized to the same expression scale. Relative expression module scores are depicted with red being higher expression and blue being lower expression.

Fig. S22

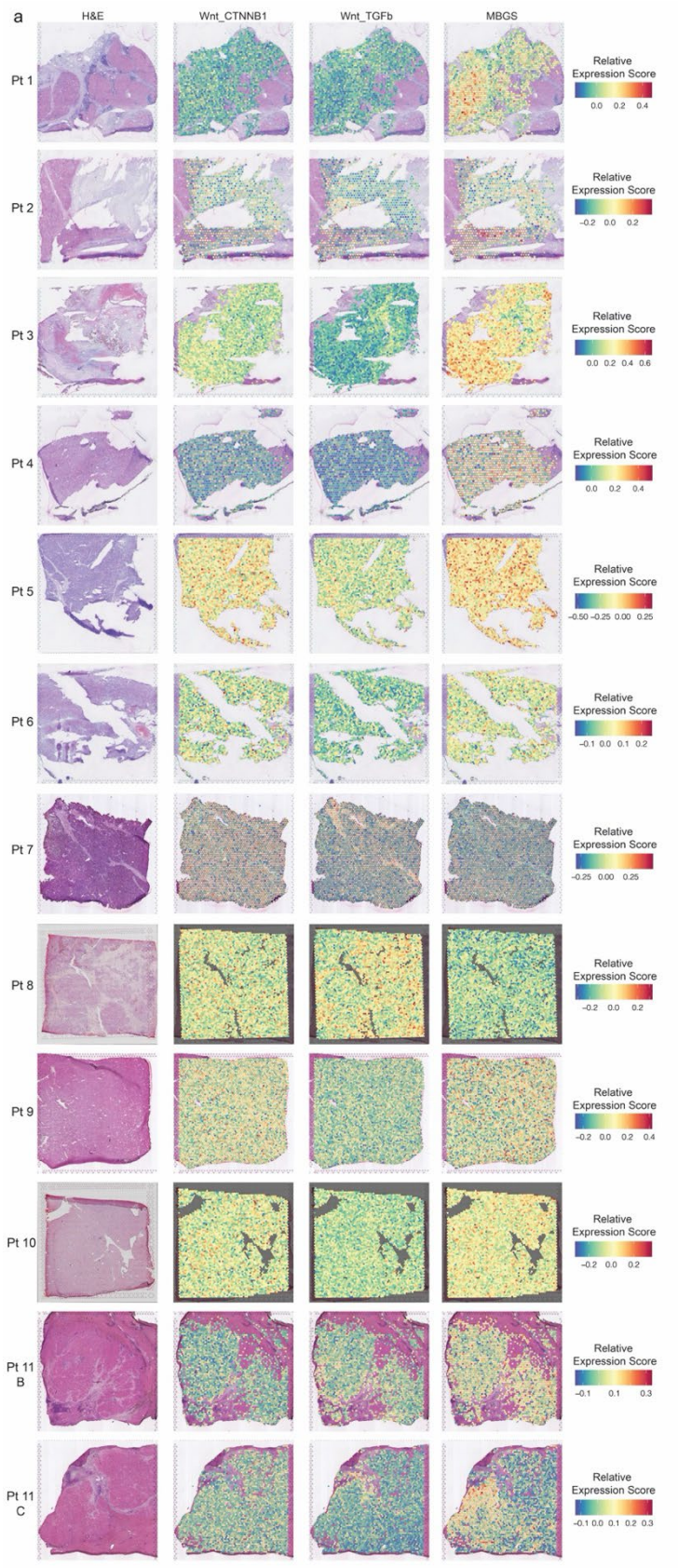
a
H&E
Wnt_CTNNB1
Wnt_TGFb
MBGS
Pt 1
Pt 2
Pt 3
Pt 4
Pt 5
Pt 6
Pt 7
Pt 8
Pt 9
Pt 10
Pt 11 B
Pt 11 C
Relative Expression Score
0.0 0.2 0.4
−0.2 0.0 0.2
0.0 0.2 0.4 0.6
0.0 0.2 0.4
−0.50 −0.25 0.00 0.25
−0.1 0.0 0.1 0.2
−0.25 0.00 0.25
−0.2 0.0 0.2
−0.2 0.0 0.2 0.4
−0.2 0.0 0.2
−0.1 0.1 0.3
−0.1 0.0 0.1 0.2 0.3

Fig. S22. Expression of Lachenmayer Wnt molecular subclassification onto spatial transcriptomic tissue section compared to MBGS. 11 (12 total slides) patient slides with H&E are shown with expression of various subclassification gene signatures shown with each spot. All the slides are normalized to the same expression scale. Relative expression module scores are depicted with red being higher expression and blue being lower expression. Pt 3 and Pt 11C slides are shown in **Fig. 8b**, but are depicted also here again to show as part of the total cohort analyzed.

Fig. S23

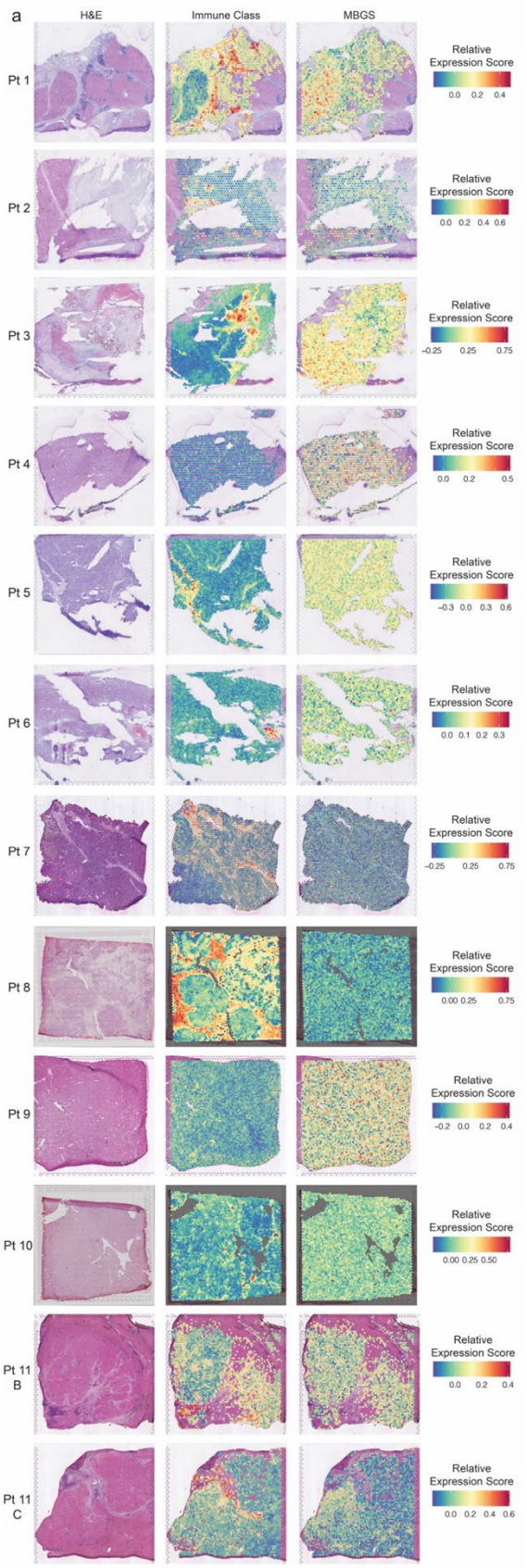
a
H&E
Immune Class
MBGS
Pt 1
Pt 2
Pt 3
Pt 4
Pt 5
Pt 6
Pt 7
Pt 8
Pt 9
Pt 10
Pt 11 B
Pt 11 C
Relative Expression Score
0.0 0.2 0.4
0.0 0.2 0.4 0.6
−0.25 0.25 0.75
0.0 0.2 0.5
−0.3 0.0 0.3 0.6
0.0 0.1 0.2 0.3
−0.25 0.25 0.75
0.00 0.25 0.75
−0.2 0.0 0.2 0.4
0.00 0.25 0.50
0.0 0.2 0.4
0.0 0.2 0.4 0.6

Fig. S23: Expression of Sia immune subclass molecular subclassification onto spatial transcriptomic tissue section compared to MBGS. 11 (12 total slides) patient slides with H&E are shown with expression of various subclassification gene signatures shown with each spot. All the slides are normalized to the same expression scale. Relative expression module scores are depicted with red being higher expression and blue being lower expression. Pt 1 and Pt 3 slides are shown in **Fig. 8c**, but are depicted also here again to show as part of the total cohort analyzed.

Supplementary tables

Table S1-S8: Attached as Excel spreadsheet as an independent document.

Table S9. Gene signatures of existing HCC classifiers.

Table: Gene Signatures		
Gene Signature	**Gene List**	**Citation**
Hoshida S1	"ACP5","ACTA2","ADAM15","ADAM8","ADAM9","AEBP1","AIF1","AKT3","ALDOA","ALOX5AP","ANXA1","ANXA4","ANXA5","AP2S1","AQP1","ARF5","ARHGDIB","ARPC1B","ARPC2","ASAH1","ATP1B3","ATP6AP1","ATP6V0B","ATP6V1B2","ATP6V1F","BCL2A1","BLVRA","C1QB","C3AR1","CAPZA1","CBFB","CCL3","CCL5","CCN1","CCN2","CCND2","CCR7","CD151","CD37","CD3D","CD47","CD48","CD53","CD74","CD8A","CDC20","CDC25B","CDH11","CDK2AP1","CELF2","CHN1","COL11A1","COL15A1","COL1A2","COL3A1","COL4A1","COL4A2","COL5A2","COL6A1","COL6A2","CORO1A","CRABP2","CRIP2","CSRP3","CTSC","CTSS","CXCL1","CXCR4","CYBA","CYBB","CYFIP1","CYP1B1","DAB2","DCTN2","DDR1","DDR2","DDX11","DGKA","DGKZ","DNM2","DPYSL2","DUSP5","DUT","EFEMP1","EFNB1","F13A1","FBN1","FBRS","FCGBP","FCGR2A","FGL2","FHL3","FLNA","FUT4","FYB1","GEM","GLIPR1","GNAI2","GNS","GPNMB","GRN","GSTP1","GUCY1A1","GYPC","HCLS1","HEXA","HIF1A","HK1","HLA-DMA","HLA-DOA","HLA-DPB1","HLA-DQA2","HLA-DQB1","ID3","IER3","IFI16","IFI30","IGFBP5","IGKC","IGLL1","IKBKE","IL15RA","IL2RB","IL2RG","IL7R","IQGAP1","IRF1","ITGB2","ITPR3","KLC1","KLF5","LAMB1","LAPTM5","LCP1","LDHB","LGALS1","LGALS3BP","LGALS9","LGMN","LHFPL2","LITAF","LMO4","LOX","LSP1","LTBP2","LTBP3","LTF","LUM","LYN","M6PR","MAP1B","ME1","MFAP1","MGP","MPHOSPH6","MSN","MTHFD2","MYCBP2","NBL1","NPC2","NSMAF","OAZ1","PAK1","PAM","PAPSS1","PCLAF","PEA15","PFN1","PGK1","PIM2","PKD2","PKMYT1","PKN1","PLAUR","PLD3","PLP2","PNP","POLD3","POSTN","PPIC","PPP1CB","PPP4C","PPP4R1","PRKD2","PRMT5","PROCR","PSMD2","PTPRC","PYGB","QSOX1","RAB31","RALB","RALGDS","RCC1","RHOA","RIN2","RIT1","RNASE1","RNASE6","RPA2","RSU1","S100A10","S100A11","S100A13","SLA","SLBP","SLC1A5","SLC2A1","SLC2A5","SLC39A6","SLC7A5","SMAD2","SMARCD1","SPAG8	Hoshida[8]

	","SRGN","SRI","STK38","STX3","TAGLN","TAX1BP3","TCF4","TFF3","THY1","TIMP2","TMSB4X","TNFRSF1B","TP53BP1","TPM2","TRAF3","TRAF5","TRIP10","TSPAN3","TUBA4A","VCAN","ZNF384"	
Hoshida S2	"ABCB10","ABCD3","ACP1","ADD3","AFP","AHCY","ARHGAP35","ARID3A","ATF2","ATM","ATP2B1","ATP2B2","ATP5PB","ATXN10","BCAM","BCLAF1","BRD3","BTG3","CASC3","CD46","CDK6","CHKA","CLK2","COL2A1","CPD","CSE1L","CSNK2A1","CSNK2A2","CTNNB1","CUL4A","CXADR","DDX1","DDX18","DEK","EIF4A2","EIF4B","ENPP1","EP300","ERBB3","FBL","FGFR3","FGFR4","FLNB","GBF1","GCN1","GLUD1","GNAI1","GPC3","GTF2I","GTF3C2","H1-0","HELZ","HMGCR","HNRNPA2B1","HNRNPC","HNRNPU","IDI1","IGF2","IGF2R","ITIH2","KLF3","LBR","MAPK6","MEST","NCOA4","NET1","NR2C1","NR5A2","NREP","NT5E","NUP153","PEG3","PHF3","PHKA2","PIGC","PLXNB1","PNN","POFUT1","PPARG","PPP2R1A","PRDX3","PTOV1","RAB4A","RBM39","RPL24","RPL27","RPL31","RPS19","RPS24","RPS25","RPS27","RPS5","RRP1B","SEPHS1","SLC6A2","SLC6A5","SMARCA1","SMARCC1","SNRPE","SNTB1","SREBF2","SSB","SUMO1","SUZ12","TARBP1","TBCE","TFIP11","TIA1","TIAL1","TM9SF4","TP53BP2","TPR","TRIM26","TTC3","UBE2K"	Hoshida[8]
Hoshida S3	"ABCB4","ABCC6","ABHD2","ACAA2","ACADM","ACADS","ACADSB","ACADVL","ACO1","ACOX1","ACOX2","ACSL1","ACY1","ADA2","ADH4","ADH6","ADK","AGL","AGXT","AKR1C1","ALAS1","ALDH1A1","ALDH1B1","ALDH2","ALDH3A2","ALDH4A1","ALDH6A1","ALDH7A1","ALDOB","ALPL","AMFR","AMT","ANXA6","AOC1","APCS","APOA1","APOC2","APOC4","APOH","AQP7","ARG1","ARHGEF12","ARSA","ASCL1","ASGR1","ASGR2","ASL","ASS1","ATOX1","ATP5F1D","ATP5PF","AZGP1","BAAT","BDH1","BHMT","BLOC1S1","BLVRB","BPHL","BTD","C1R","C1S","C4A","C4BPA","C8B","CA2","CAT","CBR1","CD14","CD302","CD81","CES1","CFB","CFH","CGREF1","CNGA1","COL18A1","COX5B","CP","CPA3","CPA4","CPB2","CPS1","CRABP1","CRYAA","CRYM","CSTB","CTH","CTSO","CXCL2","CYB5A","CYFIP2","CYP21A2","CYP27A1","CYP2C9","CYP2J2","CYP3A7","DAO","DCAF8","DECR1","DNASE1L3","DPAGT1","DRG2","ECHS1","ECI1","EDNRB","EGFR","EHHADH","EMP2","EPAS1","EPHX1","ETS2","F11","F2","F5","FAH","FANCA","FGB","FGG","FH","FKBP2","FLT4","FMO4","FOXO1","FXR2","GCH1","GCHFR","GCKR","GGH","GHR","GJB1","GLYAT","GOT2","GPT","GPX2","GPX3","GSTA2","GSTO1","GSTZ1","HAAO","HADH","HGD","HMGCS2","HMOX2","HPD","HRG","	Hoshida[8]

	HSD17B10","HSD17B4","ICAM3","IDH2","IDH3A","IFIT1","IGF1","IL13RA1","IL32","IL6R","IMPA1","INSR","IQGAP2","ISG15","ITIH1","ITIH3","ITIH4","ITPR2","IVD","KCNJ8","KLKB1","KMO","KNG1","LCAT","LONP1","LPIN1","LPIN2","MAOA","MAOB","MAPRE3","MGST2","MME","MMUT","MSMO1","MT2A","MTHFD1","MTHFS","MYLK","MYO1E","NDUFV2","NFIB","NFIC","NFKBIA","NHERF2","NNMT","NRG1","PAH","PAPSS2","PCCA","PCCB","PCK1","PCK2","PDK4","PGM1","PGRMC1","PIK3R1","PKLR","PLA2G2A","PLCG2","PLG","PLGLB2","PNPLA4","POLD4","PON3","PPP2R1B","PROS1","PTGR1","PTS","QDPR","RARRES2","RBP5","RGN","RHOB","RIDA","RNASE4","SBDS","SDC1","SDHB","SDS","SELENBP1","SELENOP","SERPINA3","SERPINA6","SERPINC1","SERPING1","SHB","SHMT1","SLC10A1","SLC16A2","SLC23A1","SLC23A2","SLC2A2","SLC35D1","SLC6A1","SLC6A12","SLC7A2","SLCO2A1","SLPI","SMARCA2","SOAT1","SOD1","SOD2","SORL1","SPAM1","SPARCL1","SRD5A1","SREBF1","SULT2A1","TCEA2","TDO2","TGFBR3","TINAGL1","TJP2","TMBIM6","TMOD1","TOB1","TPMT","TST","UQCRB","VSIG2","ZNF160"	
Chiang CTNNB1	"AADAC","ABCB11","ABCG2","ABHD6","ACE2","ACSL5","ACSL6","ACSM3","ACSS3","ACTN2","ADH6","ADRB2","ALDH1L1","ALDH3A1","ALDH3A2","AMACR","ANKFN1","AOX1","AQP11","AQP6","AQP9","AR","ASAP2","ASPSCR1","AXIN2","BAMBI","BHLHE40","BIK","BMP4","BOK","C1orf112","C1orf53","C20orf204","C3orf85","CAP2","CAVIN2","CCDC170","CD36","CDC14B","CDK6","CLDN2","CORIN","CPPED1","CRLS1","CST1","CTNNA2","CTNNBL1","CYP1A1","CYP2E1","CYP8B1","DCXR","DNAJC12","DPP4","DSG1","DYNC1I1","EBPL","ECM2","EPHB2","ESRRG","EXPH5","FAM169A","FAM3B","FAM8A1","FAS","FGF13","FITM2","FRMD3","GFRA1","GLUL","GLYAT","GNAI1","GPAM","GPHN","GRHPR","GRK3","GSTM2","H2AC8","HABP4","HEPACAM","HHAT","HIBADH","HLF","HOGA1","HPD","HSD11B1","HSDL2","HTR2B","INSIG2","IRS1","IRX3","ITPR2","KCNJ8","KCNK1","LGR5","MAP3K8","MERTK","MME","MTHFD1","MYRIP","NAGS","NEK3","NKD1","NUBPL","NUDT6","PAGE4","PANX1","PDK1","PDK4","PHLPP1","PHYHIPL","PLAAT2","PLPPR1","PRAG1","PREB","PRR5L","PTPRG","RAB11FIP2","RBP1","REG1A","REG3A","RHBG","RHOBTB1","RTP3","RUNDC3B","SALL1","SEC14L2","SELENBP1","SEPTIN4","SHLD2","SLC13A3","SLC16A1","SLC16A10","SLC16A11","SLC16A4","SLC17A1","SLC1A2","SLC22A11","SLC22A4","SLC25A30","SLC2A12","SLC47A1","SLC4A4","SLC5A6","SLC6A12","SLCO1B1","SMPX","SNAI2","SPARCL1","SPRYD7","SRD5A2","SULT1B1","TAPT1-	Chiang[9]

	AS1","TBCK","TBX3","TENM2","THBS4","TMEM100","TMEM150C","TMEM245","TMEM64","TNFRSF19","TPRG1","TRIB2","TSPAN5","TTC30A","TTC9","TTPA","UBXN10","UST","VEGFD","VLDLR","WASHC3","YPEL1","ZNF385B","ZNRF3"	
Chiang IFN	"ACSL4","ALOX5AP","APOF","CALCRL","EVI2A","FCGR2B","FCGR3A","GOT1","GPR65","HPGD","IFI27","IFI6","ISG15","KCNT2","KLRB1","KMO","MOXD1","MS4A4A","NNMT","PLA2G2A","PRAMEF10","SERPINA7","SLC12A2","SLC38A4","STAT1","TDO2"	Chiang[9]
Chiang Polysomy7	"AADACP1","ABCB4","ADAMTS17","ADCY1","ADSS1","ANO1","ARMC6","AZGP1P2","CDHR3","CHAC1","CHN2","CIDEB","CLDN14","CLDN15","CLDN3","COBL","CROT","CRYAA","CYP2A6","CYP2A7","DAO","DHRS1","ELAVL1","EPHA1","FBXO2","FCGRT","FNDC5","FOLH1","GARNL3","GCGR","GCK","GLCCI1","GPR88","H2AZ2P1","HAAO","HAPLN4","ICA1","IGFALS","LAMB3","LINC01018","LRRC31","MAD1L1","MAGEB2","MAP1LC3A","MFSD2A","MNS1","MOGAT3","MPND","MPPED1","NLRP11","PEMT","PEPD","PFKFB1","PILRB","POLD2","POR","POT1","PRKAG2","PRSS8","PTK6","PYGL","RAPGEF4","RHOU","SHC4","SLC16A2","SLC22A1","SLC25A47","SLC28A1","SRD5A1","SYTL4","TKFC","TLE2","TM6SF2","TMEM139","TRIM35","TSPAN33","TUBE1","WNK3","ZSCAN21"	Chiang[9]
Chiang Proliferation	"ABCC1","AFP","ANLN","ARHGAP18","ARID3A","ASPM","ASRGL1","ATP1A1","AURKA","AURKB","B3GNT5","B4GALT5","BACE2","BARD1","BCAT1","BIRC5","BUB1B","CCNA2","CCNB1","CCNB2","CCNE1","CD24","CDC20","CDC6","CDC7","CDCA5","CDCA7","CDCA7L","CDK1","CDKN3","CENPE","CENPF","CENPK","CEP55","CHST11","CKAP2L","CKAP4","CMTM3","CTBP2","CYBA","DBN1","DDR1","DEPDC1","DEPDC1B","DLGAP5","DSCC1","DTL","DUSP9","E2F8","ECT2","ELF4","ELOVL7","ETV4","EZH2","FAM118A","FANCI","FBXO5","FDCSP","FEN1","FHOD3","FLVCR1","FMNL2","FOXM1","FUNDC1","G6PD","GALNT7","GLIS2","GPD1L","H19","H4C3","HDAC2","HELLS","HJURP","HK2","HMGB2","IGF2BP3","JPT1","KIF11","KIF14","KIF18B","KIF20A","KIF23","KIF2C","KIF4A","LAMB1","LDLRAD3","LHFPL2","LMNB1","LRRC1","MAD2L1","MAPK13","MARCHF3","MARCKS","MARCKSL1","MCM2","MCUB","MECOM","MEP1A","MKI67","MMD","MMP12","MMP9","MTMR2","NCEH1","NCK2","NDC80","NEK2","NT5DC2","NUF2","NUSAP1","OIP5","ORC6","P3H4","PAFAH1B3","PAG1","PAPLN","PBK","PDE9A","PELI1","PIGAP1","PKDCC","PKM","PLBD1","PLP2","PM20D2","PNMA1","POU2AF3","PRC1","P	Chiang[9]

	RKCD","PRR11","PTP4A3","PTTG1","RACGAP1","RAD51AP1","RFC4","RMI2","S100P","SALL2","SALL4","SASS6","SEL1L3","SELENOM","SGO2","SHCBP1","SKA1","SLAMF8","SLC16A3","SLC1A5","SLC38A1","SLC39A10","SLC7A7","SMC4","SOX4","SOX9","SPHK1","SYNJ2","TAP1","TMED3","TMEM51","TMEM65","TNFRSF21","TOP2A","TPX2","TRIP13","TRNP1","TSC1","TTF2","TTK","TUBA4A","UBE2C","UGCG","VEGFB","WASF1","WSB1","YBX3","ZC2HC1A","ZFAS1","ZNF532","ZWINT"	
Chiang Unannotated	"ABCA9","ACOX1","ARHGEF1","ARHGEF10L","ARMC8","ARNT","B2M","B4GALT1","BACH2","BHMT","CDK13","CFHR3","CP","CPEB4","CYP1A2","CYP2A7","CYP2B7P","CYP2C19","CYP4A11","DOCK5","DPYS","DUSP16","EGR1","ELL2","ETS2","F11","FCN3","FOSB","FTCD","GLS2","GPAT3","GSAP","GSDMB","HGFAC","HSDL2","HSPD1","ID2","IDO2","KANSL1","KIFC3","LEPR","LINC01554","LMO7","LPA","LRP6","LRRFIP2","LURAP1L","MAP3K13","MARVELD2","MBNL2","MUC20","NAMPT","NBPF11","NCOA2","NSUN6","PALM3","PCSK6","PIK3R1","PITPNB","PLG","PROZ","RAPGEF2","RNF125","RORA","SERPINB9","SIK3","SLC20A1","SLC22A3","SLC25A18","SLC25A47","SLC39A14","SLX4IP","SMIM14","SMURF1","SORBS2","SORL1","SRSF4","THBS1","TMEM178A","TNFSF14","TNRC6A","TPCN2","TRIR","UBE2B","WWC1","ZFAND5"	Chiang[9]
Boyault G1/G2	"AFP","ARF1","ATRN","CAMSAP2","CEBPA","CHKA","CREB3L2","EFNA1","FBXW2","FGFR4","GORASP2","H1-0","HSPA14","LPGAT1","MFF","MKKS","MYH4","NCK2","NUAK1","PIGC","PRCC","RAP2A","RBM34","RCOR3","RPS6KC1","SCAMP3","SLC29A1","SMYD3","SUN1","SYNJ2","TMEM106B","TMEM183A","TMEM260","TOR3A","TTC13","TUG1","UXS1","WDR26","YY1AP1","ZNF281"	Boyault[10]
Boyault G3	"ACACA","ACTL6A","ADSL","AGA","AIMP1","ANP32E","ARPC4","ARPP19","ASAP1","ATIC","BOP1","BRD7","BUB1","C5orf22","CANT1","CASC3","CBX3","CCDC86","CCNA2","CCT2","CCT4","CCT5","CDC6","CENPM","CEP55","CKLF","CLIC1","COIL","COPS5","CSDE1","CSNK1D","CYB5B","DHX15","DKC1","DNAJC10","DR1","DUSP3","EBNA1BP2","EIF2S1","EIF3B","EIF3H","EIF4A3","ELOC","EMC1","EML4","ENO1","ENOPH1","EZH2","FAM50A","FANCI","FNBP1L","FTH1","FXR1","G6PD","GLA","GMFB","GNB1","GNL3","GOLT1B","GPN1","GTF3C3","H2BC21","HGS","HJURP","HMMR","HNRNPR","IPO5","IPO7","ITGB1BP1","JPT1","KDM3A","KIF1B","KIF2A","KIF2C","KLC1","KPNB1","LANCL1","LPCAT1","LRP12","LRRC59","MAD2L1","MAPRE1","MARCKS	Boyault[10]

	","MED1","MED24","MELK","MMD","MPV17","MPZL2","MRPL42","MRTO4","NARS1","NCAPD2","NCAPG","NDC1","NDC80","NDRG1","NGRN","NLE1","NME1","NME2","NOL11","NPEPPS","NRAS","NSF","NTAQ1","NUP107","NUP155","NUP37","PAK1IP1","PAPOLA","PDCD2","PFN2","PGD","PGK1","PHB1","PHLDA2","PIGF","PLEKHF2","PLOD2","POLR2K","PPP1CC","PPP2R3C","PRIM1","PRKAR1A","PRMT5","PSMC4","PSMC6","PSMD11","PSMD14","PSME3","PTBP2","PTGES3","PTP4A2","PUS7","PWP1","RAD21","RAD51AP1","RBBP4","RBM28","RFC3","RIT1","RPL8","RPRD1A","SAP30BP","SEC61G","SLC16A3","SLC38A6","SLC52A2","SLC7A1","SMAD2","SMC1A","SMG8","SNRPA1","SNRPD2","SNX7","SRI","SRM","STMN1","SUB1","TACC3","TAF2","TBL1XR1","TDG","TGIF1","TIPIN","TMEM185B","TMX1","TOPBP1","TPD52","TPD52L2","TPRKB","TRIM31","TRIP13","TSN","TTK","TXN","UBE2V2","UBR5","UCK2","UGCG","USP14","USP3","UTP18","VMP1","WASHC5","WDR12","WDR45B","XPO1","ZWILCH"	
Boyault G5/G6	"CPPED1","DPP4","DUT","GLUL","LAMA3","NEDD4","REG3A","RHBG","SMYD2","SPARCL1","TBX3"	Boyault[10]
Lachenmayer Wnt-CTNNB1	"NKD1","AXIN2","ROCK2","SALL1","TLE1","DVL2","CTNNBIP1","SMAD3","TCF7","BRD7","DAAM1","CUL1","PPP3CB","DLG1","RUVBL1","TBL1XR1","SENP2"	Lachenmayer[11]
Lachenmayer Wnt-TGFb	"DAB2","PLAU","TAX1BP3","RUNX2","RAC2","FZD2","PRKCD","MMP7","PRKX","FZD7","FRAT2","CDC2","HDAC1","CACYBP","FZD6","DKK2","MVP","PRKCI","MAP1B","SFRP4","TCF4","ARRB2","CCND3","PLCB4","DKK3","ROR2","AKT3"	Lachenmayer[11]
Sia Immune Class	"NTN3","IGKC","IGKV3D-11","IGLV1-44","IGJ","CCL19","IGHG3","IGHA1","IGHM","IGHG2","IGHG1","IGHA2","IGHM","PTGDS","POU2AF1","MMP7","MGC29506","CCL18","GBP5","CD52","TRBC1","GPR171","GEM","CCL21","TARP","CXCL9","CCL2","TRBC1","IGLJ3","CHIT1","MMP9","IGL@","HLA-DRB5","CXCR4","CD8A","GZMB","LUM","TRBC2","CFTR","GZMK","CD53","PTX3","DCN","CD48","PTPRC","TRAC","FYB","AIM2","DUSP2","CYTIP","CCL5","EFEMP1","LXN","MMP12","AEBP1","IL7R","CD38","POSTN","CXCL14","FAM150B","CCL4","STMN2","C11orf96","ID4","CR2","CXCL6","FNDC1","THBS2","LTB","CLIC6","ITGB2","GZMH","CCR7","LCP2","RGS1","CD2","SMOC2","LTBP2","GZMA","COL1A2","MGP","TAGLN","CD3D","RAC2","CD27","C16orf54","S100A4","CYR61","PTGIS","COL6A3","SLA","COL1A1","MTHFD2","	Sia[12]

	SAMSN1","PMP22","SRGN","TIMP1","IGLV1-40","GABRP","CTGF","PMEPA1","C7","CORO1A","MS4A1","FAM26F","LAPTM5"	

Supplementary references

1. Tao J, Xu E, Zhao Y, et al. Modeling a human hepatocellular carcinoma subset in mice through coexpression of met and point-mutant beta-catenin. *Hepatology*. Nov 2016;64(5):1587-1605. doi:10.1002/hep.28601
2. Tao J, Krutsenko Y, Moghe A, et al. Nuclear factor erythroid 2-related factor 2 and beta-Catenin Coactivation in Hepatocellular Cancer: Biological and Therapeutic Implications. *Hepatology*. Aug 2021;74(2):741-759. doi:10.1002/hep.31730
3. Adebayo Michael AO, Ko S, Tao J, et al. Inhibiting Glutamine-Dependent mTORC1 Activation Ameliorates Liver Cancers Driven by beta-Catenin Mutations. *Cell Metab*. May 7 2019;29(5):1135-1150 e6. doi:10.1016/j.cmet.2019.01.002
4. Tao J, Zhang R, Singh S, et al. Targeting beta-catenin in hepatocellular cancers induced by coexpression of mutant beta-catenin and K-Ras in mice. *Hepatology*. May 2017;65(5):1581-1599. doi:10.1002/hep.28975
5. Goldstein LD, Lee J, Gnad F, et al. Recurrent Loss of NFE2L2 Exon 2 Is a Mechanism for Nrf2 Pathway Activation in Human Cancers. *Cell Rep*. Sep 6 2016;16(10):2605-2617. doi:10.1016/j.celrep.2016.08.010
6. Kaposi-Novak P, Lee JS, Gomez-Quiroz L, Coulouarn C, Factor VM, Thorgeirsson SS. Met-regulated expression signature defines a subset of human hepatocellular carcinomas with poor prognosis and aggressive phenotype. *J Clin Invest*. Jun 2006;116(6):1582-95. doi:10.1172/JCI27236
7. Zhu AX, Abbas AR, de Galarreta MR, et al. Molecular correlates of clinical response and resistance to atezolizumab in combination with bevacizumab in advanced hepatocellular carcinoma. *Nat Med*. Aug 2022;28(8):1599-1611. doi:10.1038/s41591-022-01868-2
8. Hoshida Y, Nijman SM, Kobayashi M, et al. Integrative transcriptome analysis reveals common molecular subclasses of human hepatocellular carcinoma. *Cancer Res*. Sep 15 2009;69(18):7385-92. doi:10.1158/0008-5472.CAN-09-1089
9. Chiang DY, Villanueva A, Hoshida Y, et al. Focal gains of VEGFA and molecular classification of hepatocellular carcinoma. *Cancer Res*. Aug 15 2008;68(16):6779-88. doi:10.1158/0008-5472.CAN-08-0742
10. Boyault S, Rickman DS, de Reynies A, et al. Transcriptome classification of HCC is related to gene alterations and to new therapeutic targets. *Hepatology*. Jan 2007;45(1):42-52. doi:10.1002/hep.21467
11. Lachenmayer A, Alsinet C, Savic R, et al. Wnt-pathway activation in two molecular classes of hepatocellular carcinoma and experimental modulation by sorafenib. *Clin Cancer Res*. Sep 15 2012;18(18):4997-5007. doi:10.1158/1078-0432.CCR-11-2322
12. Sia D, Jiao Y, Martinez-Quetglas I, et al. Identification of an Immune-specific Class of Hepatocellular Carcinoma, Based on Molecular Features. *Gastroenterology*. Sep 2017;153(3):812-826. doi:10.1053/j.gastro.2017.06.007
13. Petitprez F, Meunier L, Letouzé E, et al. MS.liverK: an R package for transcriptome-based computation of molecular subtypes and functional signatures in liver cancer. *bioRxiv*. 2019:540005. doi:10.1101/540005
14. Zhang S, Yuan L, Danilova L, et al. Spatial transcriptomics analysis of neoadjuvant cabozantinib and nivolumab in advanced hepatocellular carcinoma identifies independent

mechanisms of resistance and recurrence. *Genome Med*. Sep 18 2023;15(1):72. doi:10.1186/s13073-023-01218-y

15. Wu R, Guo W, Qiu X, et al. Comprehensive analysis of spatial architecture in primary liver cancer. *Sci Adv*. Dec 17 2021;7(51):eabg3750. doi:10.1126/sciadv.abg3750

16. Butler A, Hoffman P, Smibert P, Papalexi E, Satija R. Integrating single-cell transcriptomic data across different conditions, technologies, and species. *Nat Biotechnol*. Jun 2018;36(5):411-420. doi:10.1038/nbt.4096